https://doi.org/10.1016/j.rse.2018.12.012

An improved algorithm for retrieving the fine-mode fraction of aerosol optical thickness. Part 2: Application and validation in Asia

Xing Yan [a], Zhanqing Li [a, b*], Nana Luo [c], Wenzhong Shi [d], Wenji Zhao [e], Xingchuan Yang [e], Chen Liang [a], Fang Zhang [a], Maureen Cribb [b]

a State Key Laboratory of Earth Surface Processes and Resource Ecology, College of Global Change and Earth System Science, Beijing Normal University, Beijing, China

b Department of Atmospheric and Oceanic Science, and Earth System Science Interdisciplinary Center, University of Maryland, College Park, Maryland, USA

c Department of Geography, San Diego State University, 5500 Campanile Dr., San Diego, CA 92182-4493, USA

d Department of Land Surveying and Geo-Informatics, The Hong Kong Polytechnic University, Hong Kong, China

e College of Resource Environment and Tourism, Capital Normal University, Beijing, China

*Corresponding author:
Zhanqing Li
ESPRE/GCESS, Beijing Normal University, 19 Xinjiekouwai Street, Haidian, District, Beijing 100875, China.
Email: zli@atmos.umd.edu

Abstract

Since small aerosol particles are mostly anthropogenic, the fine-mode aerosol optical thickness (fAOT) can be used to infer $PM_{2.5}$ amounts. However, satellite-based fAOT products such as those from the Moderate Resolution Imaging Spectroradiometer (MODIS) are highly uncertain over land. An improved fAOT retrieval method called the look-up table–spectral deconvolution algorithm (LUT-SDA) was tested and improved using data from Asia. The improvement is achieved by accounting for seasonal changes instead of using constant annual mean values of the aerosol parameters used in the LUT-SDA derived from the Aerosol Robotic Network (AERONET) data from 2010 to 2014. Compared with the previous version of the LUT-SDA developed for Beijing, Hong Kong, and Osaka, the updated LUT-SDA generates more accurate fine-mode fractions (FMFs) with the total mean root-mean-square error (RMSE) decreasing from 0.24 to 0.18. The updated LUT-SDA was then applied to retrieve fAOT and was validated by retrievals from 45 AERONET sites over the period 2015 to 2016. A good accuracy was achieved by this method with 31% of the validation sites having > 50% of retrievals falling within the estimated error (EE) envelope ± (0.05 + 0.15 × AERONET fAOT) and 42% of the validation sites having 40–50% of retrievals falling within the EE envelope. In the total validation and comparison with the MODIS Collection 6 fAOT, the fAOT retrievals from the LUT-SDA agreed more closely with AERONET retrievals, showing a low bias. About 48% of the LUT-SDA-based fAOT retrievals fell within the EE envelope (RMSE = 0.29), while ~22% of the MODIS-based fAOT retrievals fell within the EE

envelope (RMSE = 0.42). The fAOT was significantly underestimated by the MODIS algorithm in most areas of Asia with many values of zero. This study demonstrates that the refined LUT-SDA method is valid for the large-scale estimation of f AOT from satellite images.

Keywords: aerosol optical thickness, fine-mode fraction, MODIS

1. Introduction

Detailed knowledge about atmospheric aerosols is essential for understanding global climate changes, air pollution, and even weather (IPCC, 2013; Li et al., 2017). Aerosol effects on Earth's radiative balance, air quality, and clouds are governed significantly by aerosol particle size (Dusek et al., 2006; Chatterjee et al., 2012). Atmospheric aerosols, particularly in the fine mode, play an important role in determining the radiation budget of the earth-atmosphere system (IPCC, 2007; Yan et al., 2014). The adverse impact of aerosols on human health is particularly susceptible to fine-mode aerosols. As such, besides the widely used aerosol optical thickness (AOT), the fine-mode AOT (fAOT) is being increasingly employed as well. Numerous studies have demonstrated that small particles such as particulate matter (PM) with a diameter < 2.5 μm, or $PM_{2.5}$, are associated with mortality, respiratory system problems, and lung cancer (Pope III et al., 2009; Gurjar et al., 2010; Beelen et al., 2014).

Particle size is one of the most important parameters to describe aerosols (Csavina et al., 2014; Mirante et al., 2014; Cheng et al., 2015; Tan et al., 2016). The fAOT is associated with the presence of fine particles emanating from anthropogenic sources and includes black carbon, organic aerosols, sulfate, and nitrate (Bellouin et al., 2005). Larger particles, or coarse-mode aerosols, are mostly emitted to the atmosphere during mechanical processes from natural sources, e.g., soil dust. The ability to distinguish between fine and coarse modes of aerosols allows us to quantify the impact of human activities on the atmospheric environment and climate. Thus, separating fine-mode aerosols from coarse-mode aerosols is the first and pivotal step for the study of anthropogenic effects on the earth's environment.

An important parameter for obtaining fAOT is the fine-mode fraction (FMF). The FMF is defined as the fraction of fAOT to the total AOT: FMF = fAOT/AOT. To date, there are two ways to determine FMF: from satellite sensors and from ground-based measurements. Kaufman et al. (2005) used Moderate Resolution Imaging Spectroradiometer (MODIS) AOT and FMF over the oceans to assess the aerosol forcing of climate which was estimated to be 1.4 ± 0.4 W m^{-2}. Although the FMF can be successfully retrieved by MODIS over oceans, it is unreliable over land. Levy et al. (2013) reported that the MODIS-retrieved FMF over land is experimental and highly uncertain. As the ratio of AOT in different spectral ranges, the FMF is more susceptible to AOD retrieval errors that are very significant in general, especially over land (Li et al., 2009; Kokhanovsky et al., 2010; Lee and Chung, 2013). In the MODIS dark target (DT) algorithm, only four aerosol modes are chosen (three

fine modes and one coarse mode) to calculate the FMF. This FMF is not a continuous variable but a value from a set of 11 discrete values ranging from 0 to 1 (Suman et al., 2014). Mielonen et al. (2011) attributed the poor MODIS FMF retrievals to the aerosol type selection. They showed that the MODIS DT algorithm over land often selects the dust aerosol model (FMF=0) for aerosol retrievals which may be an unrealistic choice in some cases. Although Levy et al. (2010) indicated that the MODIS FMF over land has little physical validity and do not recommend using it for scientific research, some attempts at using it have been made. Ramachandran (2007), for example, used the MODIS FMF to analyze its inter- and intra-annual variations over four urban areas in India. Zhang and Li (2015) proposed a physical approach of estimating $PM_{2.5}$ from the MODIS AOT, but noted that the MODIS FMF limited the application of their method, which was reinforced by Li et al. (2016).

Another way to estimate the FMF is based on ground measurements such as those made by the Aerosol Robotic Network (AERONET). The AERONET calculates the FMF using the spectral deconvolution algorithm (SDA) and provides this product at a multitude of sites around the world (O'Neill et al., 2001, 2003). Gassó and O'Neill (2006) did field experiments to test the SDA and showed a high accuracy between SDA-derived fAOT and airborne in situ measurements. As a result, the AERONET SDA product has been increasingly used by others. Arola et al. (2017) used AERONET SDA level 1 and level 2 products to assess how the fAOT is enhanced under cloudy conditions. Zhang and Li (2015) developed a relationship between the columnar volume-to-extinction ratio and the FMF based on level 1.5

SDA data from eight AERONET sites. Although AERONET sites can provide accurate FMFs, they are sparsely distributed around the world. For example, there are only a few sites in China with FMF products.

Improvements have been made to the SDA. Zhang et al. (2013) developed a parameterization scheme for correcting the fine-mode Ångström index to improve the SDA accuracy. This led to a reduction in the mean bias of the FMF from 0.072 to 0.044. An extension of the SDA into the shortwave infrared was developed by O'Neill et al. (2008) in order to enhance coarse-mode information with the aid of new AERONET instruments that included a 1.64-μm channel. This method was validated by Kaku et al. (2014). However, applying the SDA to satellite data is still a challenge. This is because the SDA needs AOT at a minimum of three wavelengths to derive the FMF. Most current satellite AOT are derived from the DT or modified DT method which can provide AOT at only the blue and red bands (Luo et al., 2015). To overcome this limitation, Yan et al. (2017a) proposed a look-up table – SDA (LUT-SDA) method that only needs AOT at two bands. It has been tested on city scales around Beijing, Hong Kong, and Osaka using MODIS data, as well as in northern China using Himawari-8 satellite data (Yan et al., 2018). The fAOT conveys more accurate information than does AOT in the estimation of surface $PM_{2.5}$ (Yan et al., 2017b). However, the original LUT-SDA was only tested on urban and regional scales, and its internal parameter was determined by annual AERONET SDA data (Yan et al., 2017a). The annual-based parameter setting in the LUT-SDA may incur significant errors because aerosol optical properties have obvious seasonal variations

(Lau et al., 2018).

The objectives of this study are: 1) to update the LUT-SDA parameters to account for the seasonal variation of aerosol properties and 2) to examine the applicability of the updated LUT-SDA for fAOT retrievals using MODIS data collected in Asia. A comprehensive discussion of the validation results and differences between the original and updated LUT-SDA retrievals as well as those using the MODIS aerosol product is presented.

2. Data and methods

2.1. Study area

Asia is currently inhabited by 60% of the world's population. With the rapid growth in population, economic development, and urbanization in Asia, air pollution has become a major environmental problem in this region (Wang et al., 2014). Asia also has diverse climatic conditions and geographic features (Fig. 1). This offers the opportunity to test the adaptability of the LUT-SDA over large spatial scales under the condition of heavy air pollution.

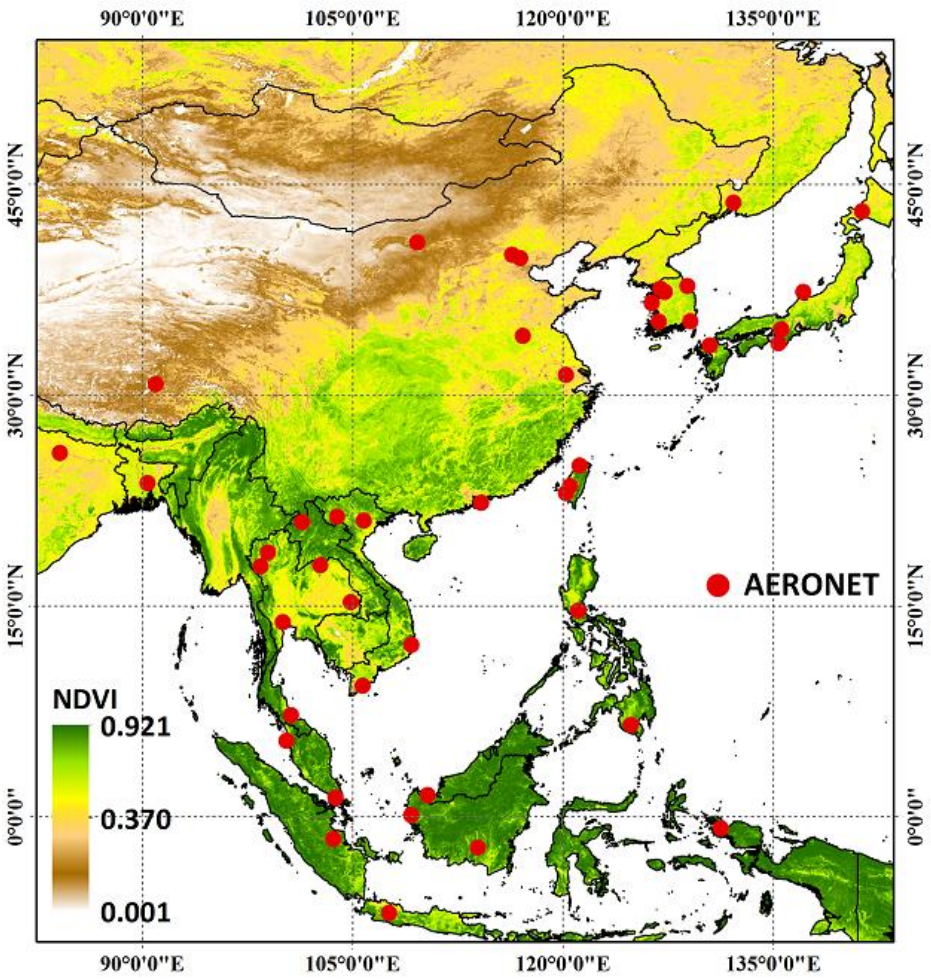

Fig. 1. The study area. Colors represent the normalized difference vegetation index (NDVI), and the red dots show the locations of AERONET sites from which data are used in this study.

2.2. MODIS data

The MODIS/Terra Level-3 (L3) Collection 6 (C6) daily gridded atmospheric data product (MOD08) from 2015 to 2016 was used for LUT-SDA fAOT calculations. The L3 MODIS aerosol product is a global daily aggregation of L2 MODIS data into grids at a spatial resolution of 1° × 1° (Hubanks et al., 2008). It is advantageous to use the MOD08 product because averaging reduces random noise, and the data quality is

checked (Suman et al., 2014). In the previous global validation, the mean error of the daily L3 MODIS 550-nm AOT is 0.03 with a root mean square error (RMSE) of 0.14 (Ruiz-Arias et al., 2013). AOTs in the channels centered at 470 nm and 660 nm were extracted from the Aerosol_Optical_Depth_Land parameter to derive the Ångström exponent (AE). The Aerosol_Optical_Depth_Land parameter is derived from the L2 MODIS aerosol product "Corrected_Optical_Depth_Land" whose quality assurance index is greater than or equal to 1 (Kokhanovsky, 2009). Since the fine-mode aerosol parameters, i.e., Optical_Depth_Ratio_Small_Land and Optical_Depth_Ratio_Small_Land_And_Ocean, were also removed from the MOD08 product (Hubanks et al., 2015), we obtained the FMF from the C6 L2 MODIS aerosol parameter (Optical_Depth_Ratio_Small_Land) and aggregated the data onto the same spatial resolution grid (1° × 1°) as the MOD08 product for comparison purposes. Note that only the DT algorithm provides FMF outputs (Levy et al., 2013). Thus, we only selected DT-based AOT and AE for this study.

2.3. AERONET

Version 2 SDA inversion products from AERONET were used. The AERONET sites chosen for this study are listed in Table S1. Level 2.0 AERONET SDA data from 2010 to 2014 in Asia were selected for examining the seasonal characteristics of the AE derivative (α'). α' is a complement to AE as a measure of the rate of slope change with respect to wavelength, which quantifies the deviation from linearity of the wavelength-based AOT variation in logarithmic coordinates (Soni et al., 2011). Level

1.5 data were used if Level 2.0 data were not available. Data from 2015 to 2016 were used for validation purposes. Since the AERONET fAOT is at 500 nm, we interpolated MODIS C6 AOT retrievals at 550 nm into 500-nm AOT for fAOT calculations and comparisons. Note that the FMF derived by MODIS is not the same quantity as that obtained from the AERONET SDA method (O'Neill et al., 2003). The AERONET SDA method assumes one coarse mode and one fine mode thus the FMF is the weighting between these two modes. However, the MODIS FMF is a weighting between bimodal models, where the fine-mode dominant models contain a coarse mode and the coarse-mode dominant models contain a fine mode. This means that the MODIS FMF is not a weighting between fine and coarse modes (Levy et al., 2007). If the MODIS FMF=0, the dust model provides the best solution for the AOT retrieval (Mielonen et al., 2011). Although the FMF is not uniquely defined, the MODIS FMF and the AERONET FMF should be correlated with each other (Jethva et al., 2007). Levy et al. (2007) validated the MODIS FMF with the AERONET FMF and showed that compared to the C5.1 FMF product, the C5.2 FMF product improved with R^2 increasing from 0.07 to 0.25. They gauged the improvement in the MODIS FMF product based on its correlation with the AERONET FMF (Levy et al., 2007).

2.4. The LUT- SDA

As described by Yan et al. (2017a), the LUT-SDA is based on the MODIS-derived AOT and AE to retrieve the FMF. To build an LUT, a set of hypothetical FMF (η) and α' are imported into the SDA along with the AE (α) to build

the relationship with the AE of the fine-mode aerosols (α_f). The LUT is thus a four-dimensional one between η, α', α, and α_f. Based on the constructed LUT, the FMF can be estimated by a cost function as shown by Yan et al. (2017a). The final fAOT is calculated using the MODIS-derived AOT and LUT-SDA-derived FMF (fAOT= AOT×FMF). In this study, we used AERONET historical SDA data to update the α' at different locations and then applied the updated LUT-SDA to retrieve fAOT. The validation domain is Asia (Fig. 2).

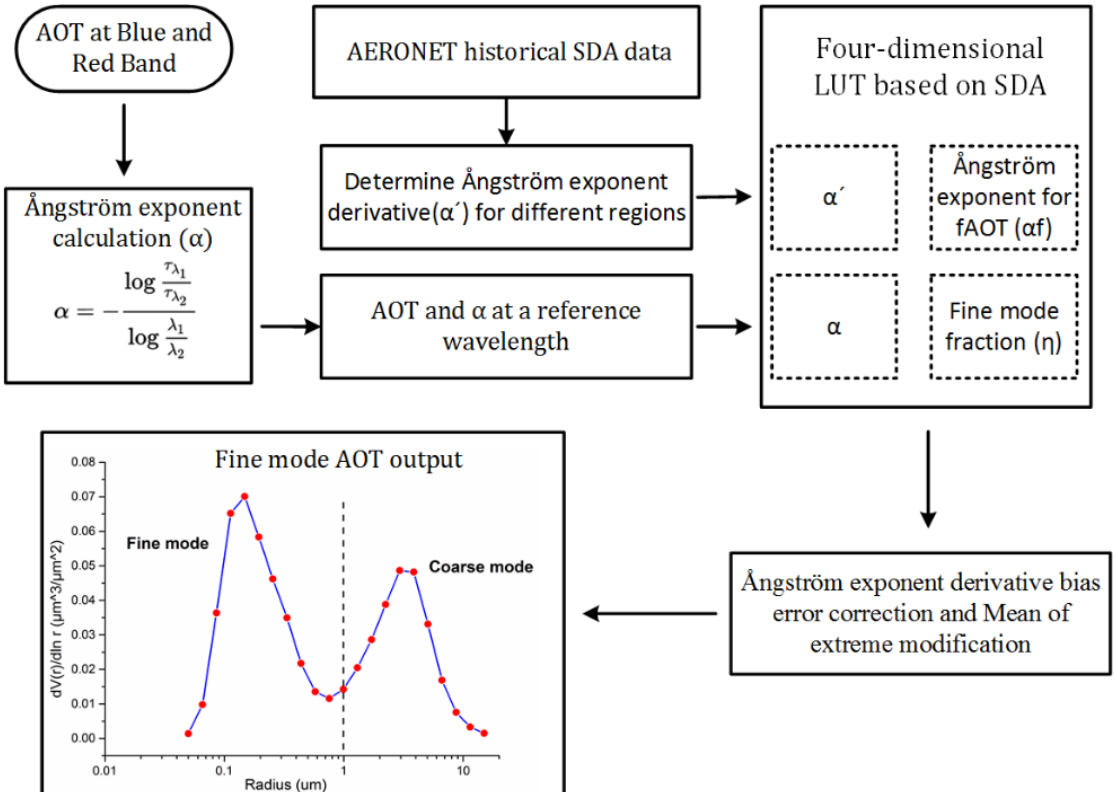

Fig. 2. Schematic diagram describing the LUT-SDA used in this study.

3. Results and discussion

3.1. Optimal seasonal AE derivative for the LUT-SDA

In the previous LUT-SDA, the α' was an annual-based setting and tested in three cities with the following ranges of values: -1.2 to 1.2 in Beijing, -0.6 to 1.8 in Hong Kong, and -0.6 to 1.4 in Osaka. However, α' contains critical aerosol particle size information, and its strong seasonal variations have been noted (Kaskaoutis et al., 2009; Soni et al., 2010; Lau et al., 2018).As shown by O'Neill et al. (2001) and Eck et al. (2010), large positive α' indicates the dominance of fine-mode aerosols whereas α' close to 0 or negative values of α' are characteristic of coarse-mode aerosols. The annual-based α' may, therefore, incur errors in the FMF retrieval and even make it hard for large scale applications.

So in this study, we further derive α' for each season in different areas of Asia. Seasonal α' values were obtained from historical data at 55 AERONET stations (Table S1). Here we used AERONET data at four sites as examples. Figure 3 reveals positive and higher values of α' at the Hong Kong Polytechnic University site (Hong_Kong_PolyU) in the spring, autumn, and winter from 2010 to 2014. This indicates that mostly fine-mode particles dominated in these seasons. However, close to 0 and negative α' are found in the summer, and its frequency is nearly the same as the positive values (values range from -2.2 to 2). This suggests the presence of both fine- and coarse-mode aerosols over Hong Kong in this season (Eck et al., 1999). Positive α' values also prevail in spring, autumn, and winter at the Chiang Mai site in

Thailand (Chiang_Mai_Met_Sta) except in summer when it is always negative. This finding is consistent with that reported by Janjai et al. (2012). Due to extensive biomass burning that occurs as a by-product of seasonal agricultural clean-up activities in the dry season (November-April), fine aerosols are more prevalent than large aerosols in spring, autumn, and winter. In Beijing and Xinglong, α' values are largely positive during summer, indicating that fine-mode aerosols dominate then. By contrast, in spring, autumn, and winter, near to 0 and negative α' values are observed, which indicates the presence of coarse-mode particles. The dominance of coarse-mode aerosols in spring was mainly attributed to the appearance of coarse mineral particles during dust events in northern China (Yu et al., 2009). Mostly fine-mode aerosols dominate during the wet season of summer in Beijing and Xinglong because of the increase in humidity and the hygroscopic growth of aerosols (Gao et al., 2013). As shown in Fig. 3, the seasonal patterns of α' at Beijing and Xinglong are similar. This suggests that α' does not change much between these neighboring cities and adjacent areas in general. Gao et al. (2013) also point out this phenomenon. That fine-mode aerosols dominate during the summer in Beijing puts into question whether Yan et al. (2017a) set an appropriate range of values for α' in their study (-1.2 to 1.2). So according to seasonal α' data at different locations, we reset the ranges of α' to be the first and third quartiles of the data in each season. Taking Beijing as an example, the range of α' is set to -0.7 to 0.6 for spring, 0.6 to 2.1 for summer, -0.7 to 1.5 for autumn, and -1 to 0.6 for winter.

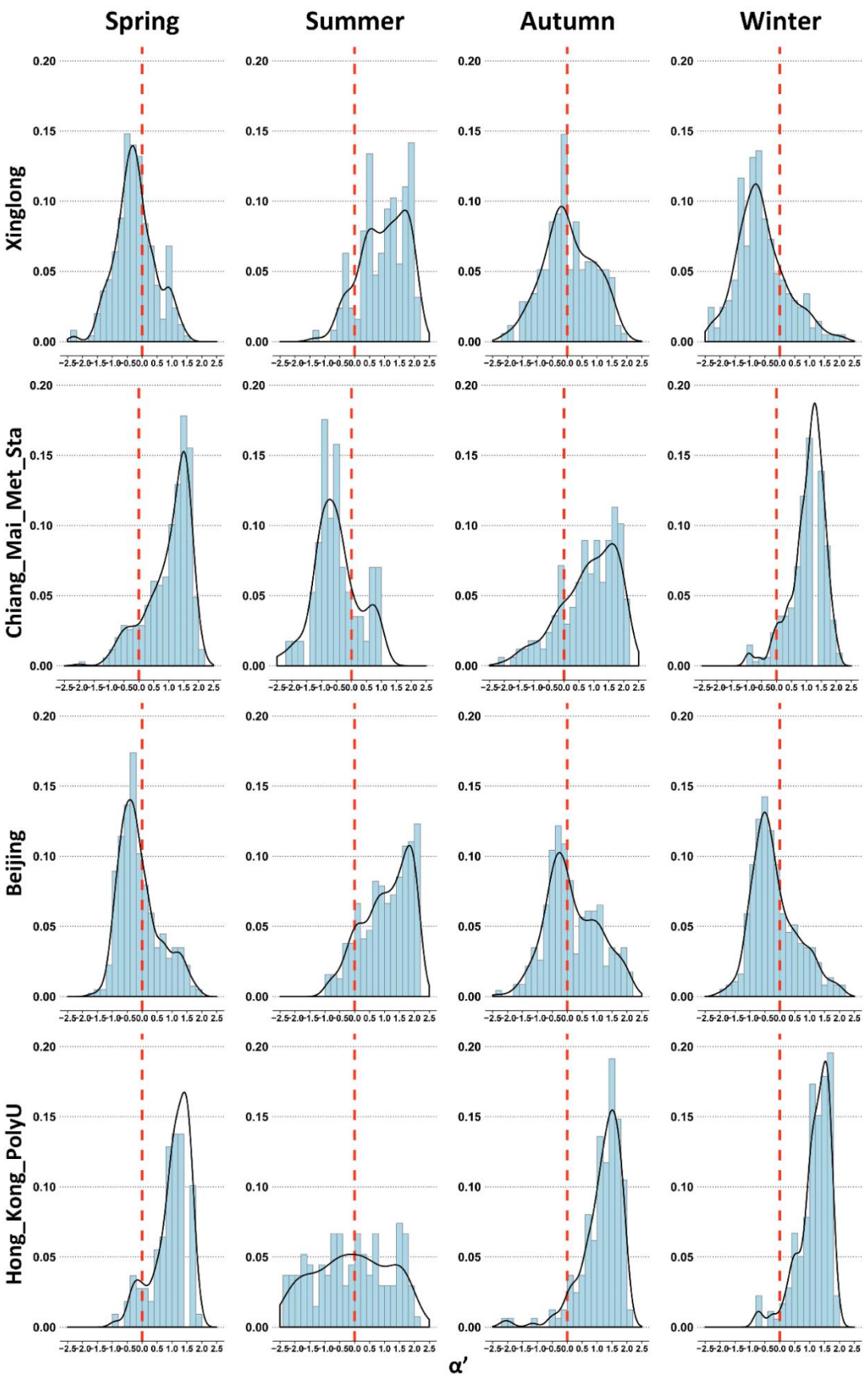

Fig. 3. Histograms of α' for different seasons at the (from top to bottom) Xinglong,

Chiang_Mai_Met_Sta, Beijing, and Hong_Kong_PolyU AERONET sites. The red dashed line shows α' = 0.

3.2 Comparison between the updated seasonal α' and annual α' for the LUT-SDA

Figure 4A-D presents seasonal LUT-SDA FMF errors arising from using seasonal α' and annual α' values for Beijing, Hong Kong, and Osaka. Figure 4D shows their RMSEs. The error is defined as the difference LUT-SDA FMF – AERONET FMF at 0.5 μm. The updated seasonal α'-based retrievals are more accurate than the annual α'-based retrievals. More of the 1-σ interval of the bias falls within the estimated error (EE) envelope in seasonal α'-based FMFs for Beijing (Fig. 4A). RMSEs are reduced in all seasons (Fig. 4D), especially in winter when the RMSE decreases from 0.29 to 0.20 (number of samples, N=71). In other words, FMF retrieval errors in Beijing in winter can be significantly reduced by using seasonal α' values instead of annual α' values. A similar reduction in retrieval errors is also seen for Osaka and Hong Kong when seasonal α' values are used instead of annual α' values. The mean RMSEs for all seasons reduces from 0.22 to 0.18 (Osaka) and 0.24 to 0.22 (Hong Kong). Overall, the total mean RMSE decreases from 0.24 to 0.18 for these three cities.

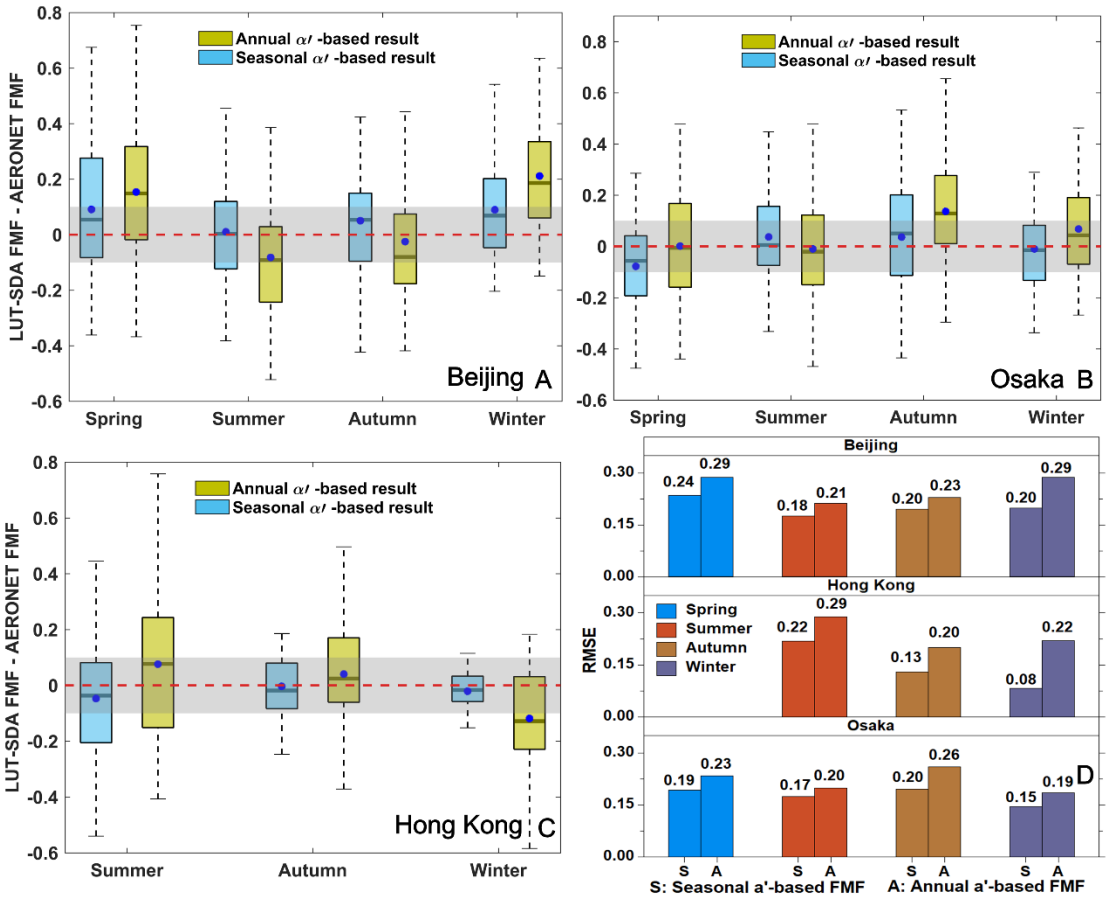

Fig. 4. FMF error as a function of season for (A) Beijing, (B) Osaka, and (C) Hong Kong. The FMF error is defined as LUT-SDA-retrieved FMF – AERONET FMF. The red dashed line is the zero-error line, and the gray shaded area is the estimated error envelope (±0.1). The means, medians, and 66% (1-σ) intervals of the differences are shown as blue dots, horizontal lines within the boxes, and the boxes themselves, respectively. The black whiskers are the 96% (2-σ) intervals. D: RMSE of the LUT-SDA FMF in different seasons using seasonal and annual α' values.

Figure 5 illustrates the improvement that occurs across the range of AERONET FMF values when using seasonal α' values. The statistics are presented as box-whisker plots where the half-widths of the blue boxes represent the standard deviations of the AERONET FMF. In Beijing and Osaka (Fig. 5A and 5C), all 1-σ

intervals of the bias, i.e., the boxes, using seasonal α' fall within the EE envelope in the AERONET FMF range of 0.6–1.0. Those using annual α' fall within the EE envelope in the AERONET FMF range of 0.7–0.9 (Fig. 5B and 5D). Compared with annual α'-based results, seasonal α'-based FMF retrievals agree better with AERONET FMF retrievals in the 0.5–1 range in Hong Kong (Fig. 5E and F). Mean biases of the seasonal α'-based retrievals are generally less than 0.1. Figure 5 also shows that there are large biases in the 0–0.5 range for both retrievals.

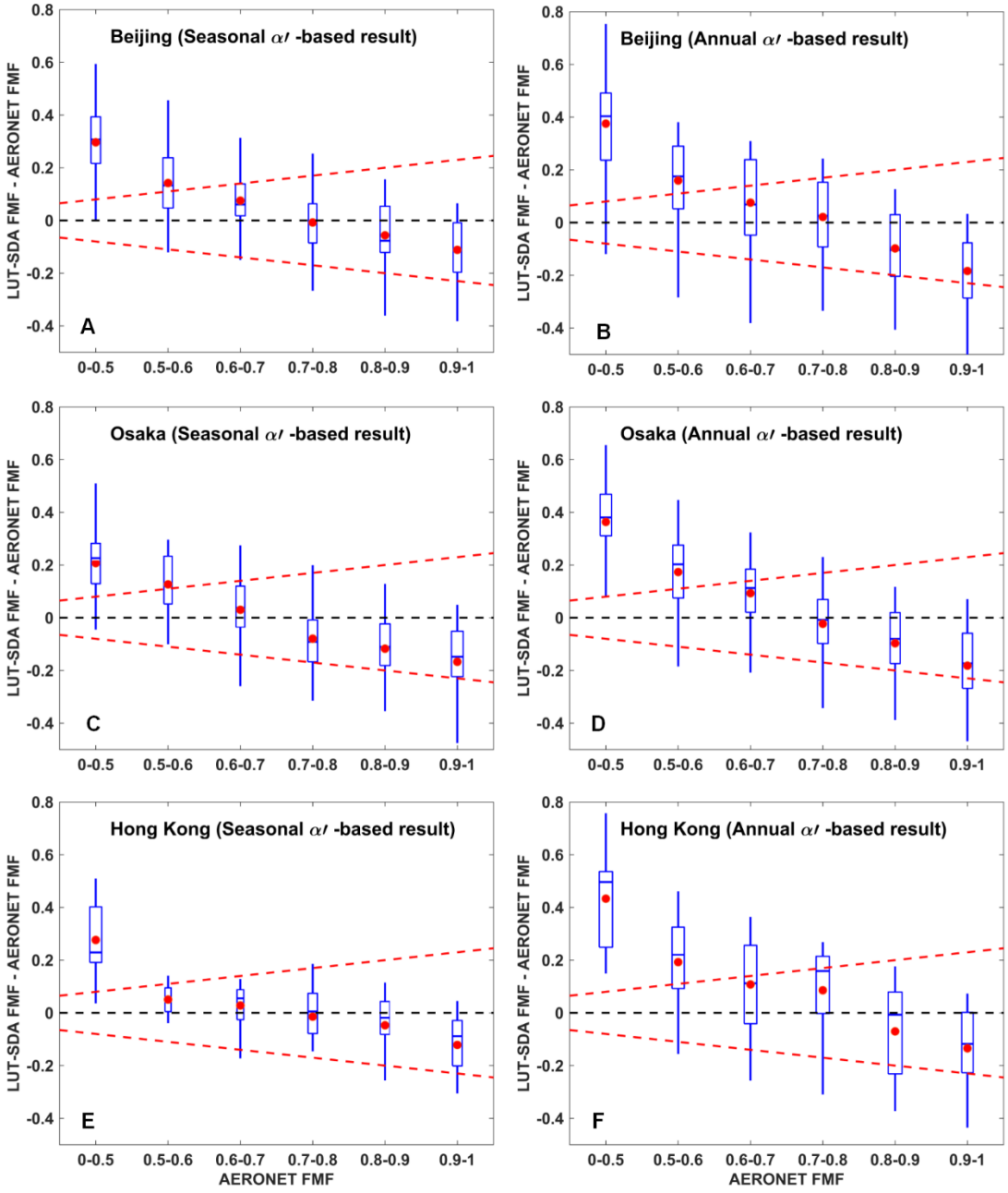

Fig. 5. Box plots of FMF errors (LUT-SDA - AERONET) as a function of AERONET

304 FMF at 0.5 μm for seasonal α'- and annual α'-based results for (A-B) Beijing, (C-D)
305 Osaka, and (E-F) Hong Kong. The means, medians, and 66% (1-σ) intervals of the
306 differences are shown as red dots, horizontal lines within the boxes, and the boxes
307 themselves, respectively. The blue whiskers are the 96% (2-σ) intervals. The black
308 dashed line is 0, and the red dashed lines represent the estimated error envelope for
309 the total FMF ± (0.05+15%).
310
311 Figure 6 shows the final fAOT calculated by seasonal α'- and annual α'-based
312 LUT-SDA FMFs for Beijing, Hong Kong, and Osaka. In Beijing, the correlation
313 between the retrieved fAOT and ground-based AERONET fAOT is improved using
314 the seasonal α' with the coefficient of determination (R^2) increasing from 0.65 to 0.69
315 and the RMSE decreasing from 0.42 to 0.39. A similar improvement is seen for Hong
316 Kong with R^2 increasing from 0.38 (from the regression of annual α'-based fAOT on
317 AERONET fAOT) to 0.49 (from the regression of seasonal α'-based fAOT on
318 AERONET fAOT). Meanwhile, the RMSE decreased from 0.27 to 0.23, and the
319 percentage of derived fAOTs within the EE envelope increased from 40% to 44%. As
320 for Osaka, again, the correlation between the LUT-SDA fAOT and the AERONET
321 fAOT is improved with R^2 increasing from 0.32 to 0.41 and the RMSE decreasing
322 from 0.16 to 0.14. Figures 4–6 confirm the validity and necessity for updated the α'
323 from the annual to the seasonal-based α' in the LUT-SDA.
324

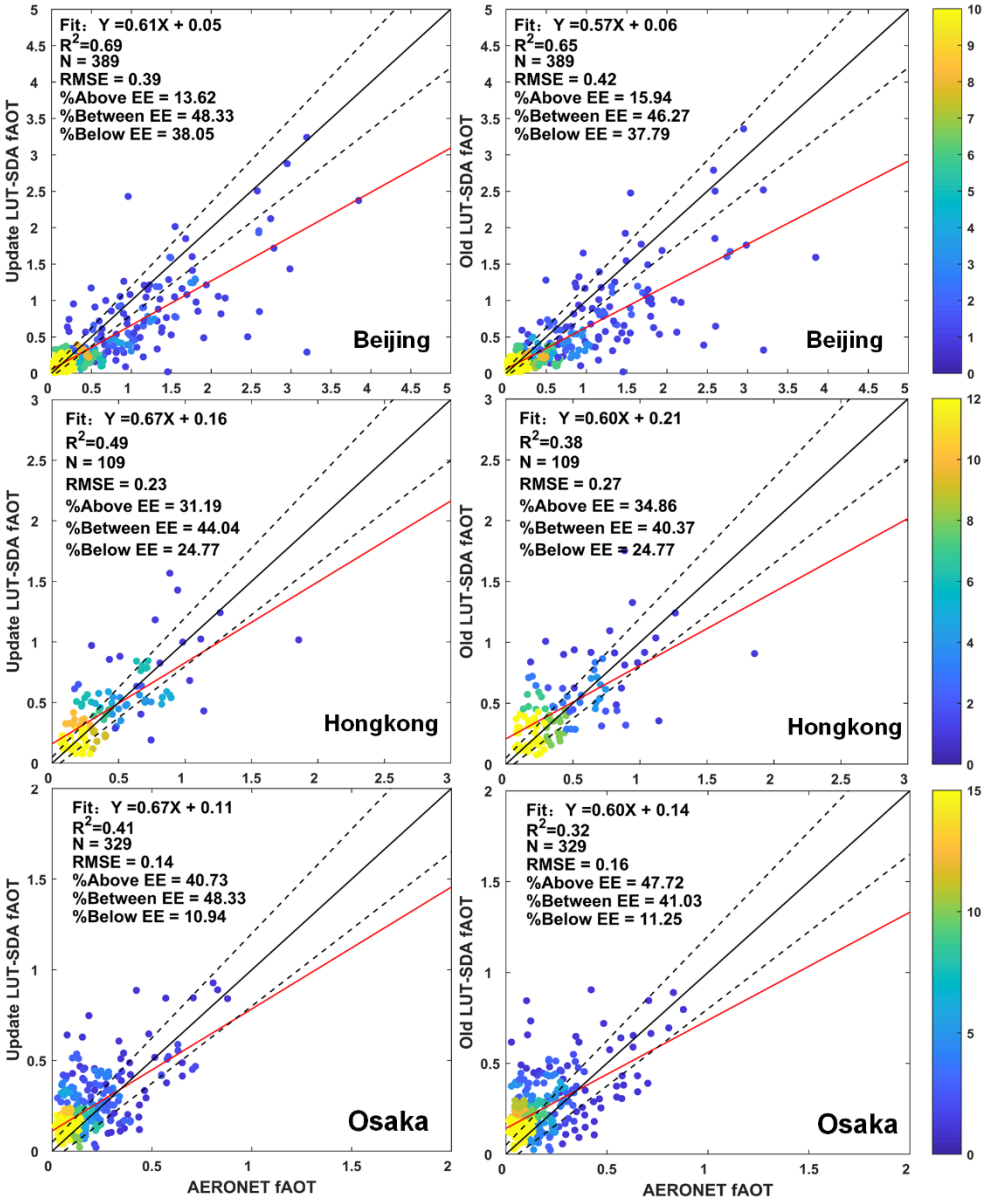

Fig. 6. Updated (seasonal α'-based, left panels) and previous (annual α'-based, right panels) LUT-SDA fAOTs collocated with 0.5-μm AERONET fAOTs. Data are sorted according to ordered pairs (AERONET, LUT-SDA) of fAOT in 0.05 intervals, and the color represents the number of cases (see color bars) having that particular ordered-pair value. The 1:1 line and estimated error (EE) envelopes ± (0.05+15%) are plotted in black solid and dashed lines, respectively. The red lines are the best-fit lines from linear regression. The coefficients of determination (R^2), the number of samples (N), and the root-mean-square errors (RMSE) are given in each panel.

3.3. Validating fAOT at different locations in Asia

Figure 7 shows seasonal mean LUT-SDA and AERONET fAOTs obtained by averaging daily fAOTs from 2015 to 2016 over Asia. In general, high fAOT loading is found in central/eastern China and northeastern India in all seasons. The population density is high, and industry is heavy in both of these regions, likely leading to the generation of anthropogenic pollution and more fine particles (Ma et al., 2014; Xin et al., 2014). In central/eastern China, the LUT-SDA fAOT in summer is higher than in other seasons. The AERONET fAOT also shows this. For example, in Beijing, the AERONET fAOT in summer (> 0.8) is higher than in spring (0.6–0.8), autumn (0.3–0.6), and winter (0.2–0.25). In summer, these regions typically experience a summer monsoon. Itahashi et al. (2012) suggested that high values of fAOT are caused by pollutant transport patterns during the monsoon in these locations. Over Bangladesh and northeastern India, the LUT-SDA fAOT reaches a maximum in winter (~1.2–2.0) and decreases in spring (~0.3–0.6). In winter in northern India, the boundary layer is shallow which gives rise to haze, leading to a higher fAOT (Ramachandran, 2007). In Vietnam, Laos, and Thailand, the LUT-SDA fAOT is highest in spring. This pattern is also seen in the AERONET fAOT dataset. Smoke aerosols due to frequent burning in spring in this region are likely responsible for this pattern. Overall, the LUT-SDA and AERONET fAOT seasonal trends and spatial patterns agree reasonably well.

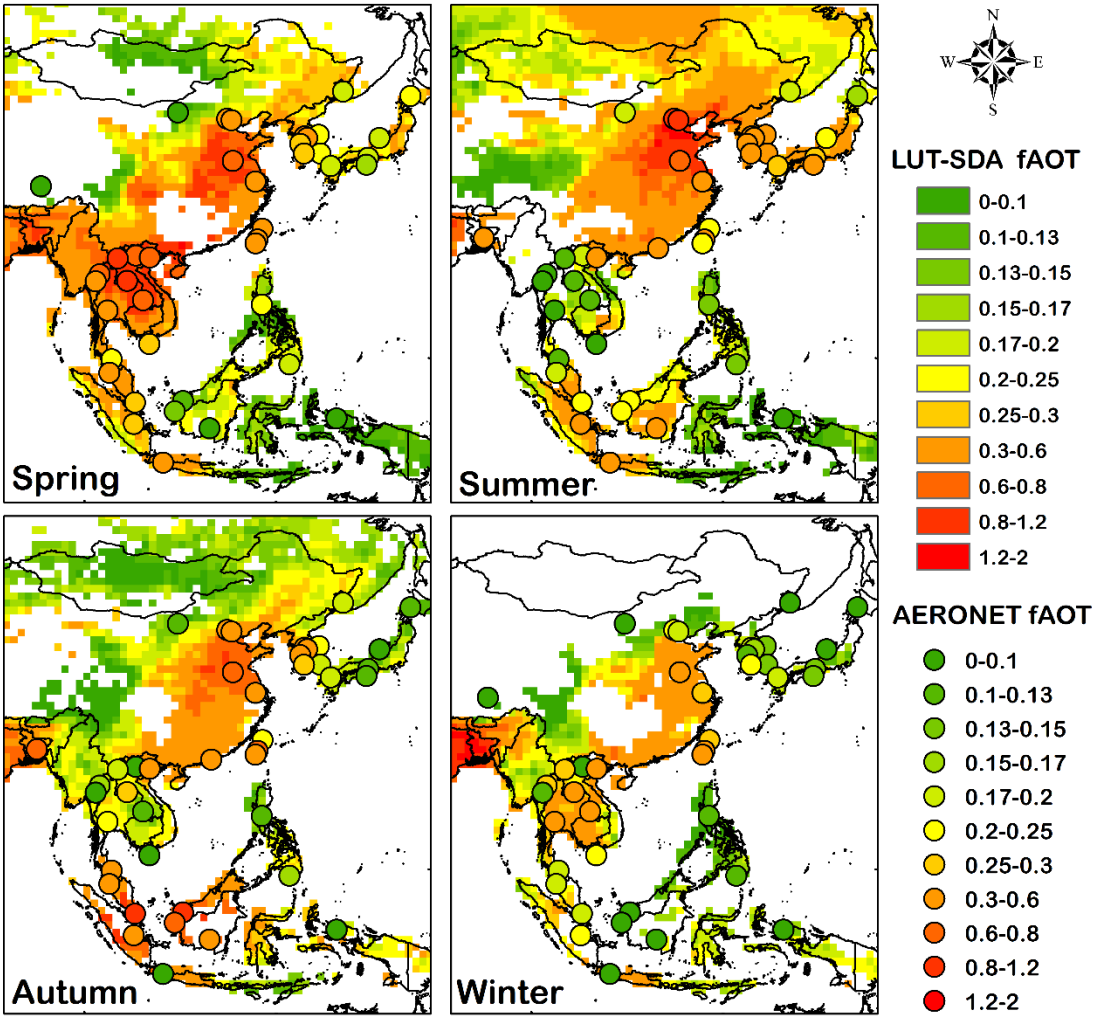

Fig. 7. Seasonal mean fAOT from the LUT-SDA (background colors) and from AERONET (colored filled circles).

Figure 8A shows validation results for all-season LUT-SDA fAOTs. The validation results for individual seasons are shown in Supplementary Fig. S1. Because the LUT-SDA fAOT is calculated as the product of the MODIS AOT and the LUT-SDA FMF, the accuracy of the MODIS AOT can have an impact on the final fAOT outputs. MODIS AOTs were thus validated using AERONET AOT retrievals (Table S2 and Figs. S2-S6). Overall, the RMSE of the MODIS AOT is 0.34 with

40.81% of the derived-AOT falling within the EE envelope ± (0.05+15%). For the LUT-SDA validation (Fig. 8A), 31% of the validation sites (the total number of validation sites is 45) have more than half of their retrievals falling within the EE envelope. Forty-two percent of the validation sites have 40–50% of their retrievals falling within the EE envelope, and 27% of the validation sites have less than 40% of their retrievals falling within this envelope. Good agreement is seen over South Korea and Japan where 40–70% of LUT-SDA retrievals fall within the EE envelope. At most validation sites in southern Asia, 30–50% of the retrievals are within the EE envelope. However, at Taihu, less than 20% of the LUT-SDA retrievals fall within the EE envelope (Fig. 8A and 8C). This is because MODIS AOT retrievals are inaccurate at this location. Fig. 8B and Table S2 shows that most of the MODIS AOT retrievals lie outside of the EE envelope at this location (N=134), and the RMSE is high (0.53). Zheng et al. (2011) suggested that the inaccurate estimation of surface reflectance is a major source of error in MODIS DT AOT retrievals. They also found that MODIS DT AOTs were significantly overestimated at Taihu, which is surrounded by parkland, with less than 30% of the retrievals falling within the EE envelope. Wang et al. (2007) and He et al. (2010) found that water pollution in Taihu Lake is the primary factor for the surface reflectance estimation error in the MODIS DT algorithm. The LUT-SDA uses MODIS AOT retrievals as input data for the FMF calculation, so the uncertainty in AOT will result in errors in the FMF outputs. Figure 8D shows that the LUT-SDA-derived FMF cannot match the AERONET FMF well at Taihu. Thus MODIS AOT retrievals are likely an important source of error in LUT-SDA retrievals

of fAOT.

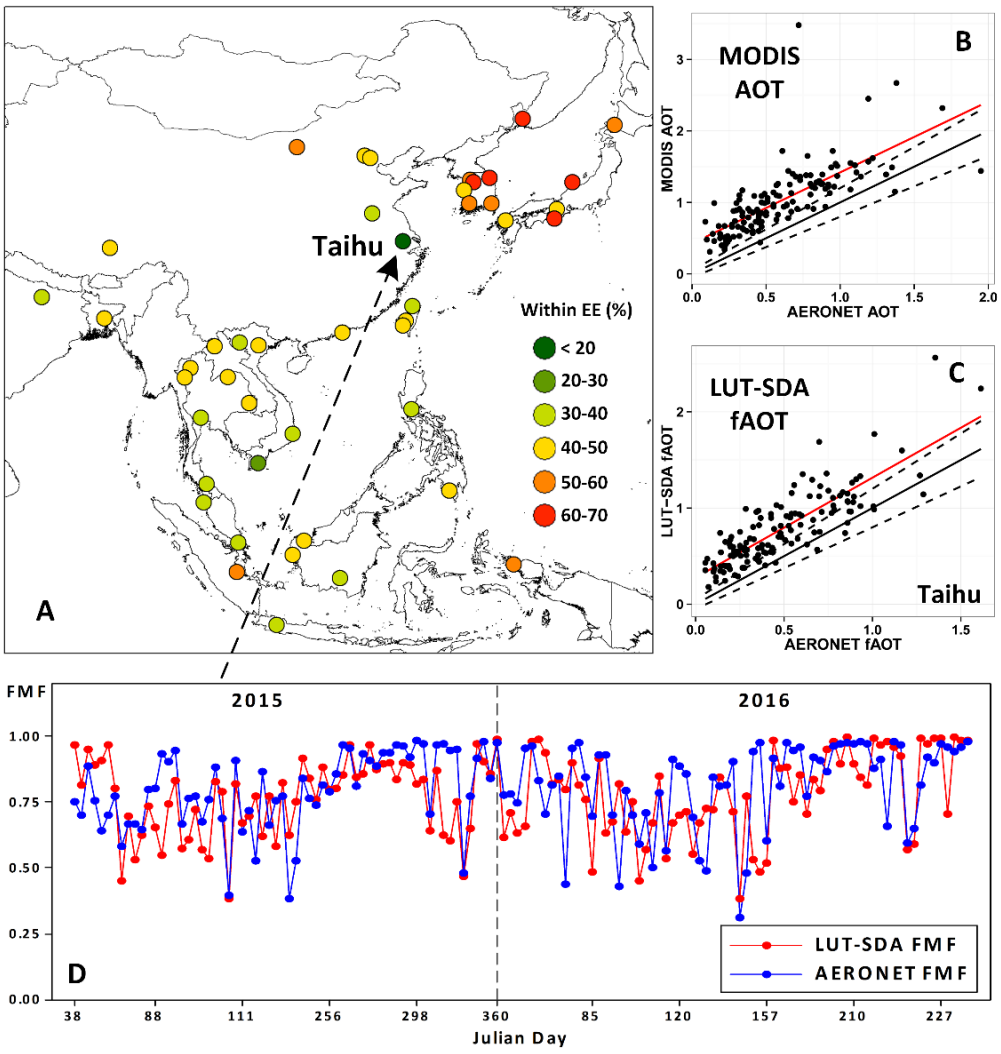

Fig. 8. (A) Validation of the LUT-SDA fAOT (at 500 nm) in Asia at each site, (B) MODIS as a function of AERONET AOT (at 500 nm) at Taihu, and (C) LUT-SDA fAOT as a function of AERONET fAOT (at 500 nm) at Taihu. The solid black lines in (B) and (C) are the 1:1 lines, the dotted black lines are the estimated error (EE) envelope lines, and the red lines are the best-fit lines from linear regression. (D) Time series of the LUT-SDA-derived FMF (in blue) and the Taihu AERONET FMF (in red) from 2015 to 2016.

399

400 *3.4. Comparison with the MODIS aerosol product*

401 Figure 9 shows yearly averaged spatial distributions of MODIS fAOT and
402 LUT-SDA fAOT. In 2015, both MODIS and LUT-SDA fAOTs were high (> 0.6) in
403 the western and northern parts of Indonesia. MODIS fAOTs ranged from 0.6–0.7 in
404 western China (Beijing, Hebei, and Shandong Province) which is much lower in
405 magnitude than the LUT-SDA fAOTs (> 0.8). An opposite pattern is seen in
406 Bangladesh where LUT-SDA fAOTs were greater than 0.8, but MODIS fAOTs ranged
407 from 0.3–0.4. In 2016, MODIS fAOTs in most parts of China were lower than
408 LUT-SDA fAOTs as well. In particular, in southern China, MODIS fAOTs ranged
409 from 0.1–0.4 while LUT-SDA fAOTs ranged from 0.5–0.7. MODIS fAOTs in
410 northern Laos are higher than the corresponding LUT-SDA fAOTs (> 0.8 and 0.6–0.7,
411 respectively). MODIS and LUT-SDA fAOTs dropped in magnitude in Indonesia and
412 slightly decreased in China in 2016 compared with the 2015 retrievals. Itahashi et al.
413 (2012) reported that the decline in fAOT corresponded to the decline in sulfur dioxide
414 (SO_2) emissions. Li et al. (2017) found that the 2016 SO_2 emission in China was 8.4
415 Mt yr^{-1} which is lower than the 2015 SO_2 emission (~10 Mt yr^{-1}). This agrees with our
416 finding of a decreasing trend in fAOT in 2016. From Fig. 9, the MODIS fAOT is
417 always lower than the LUT-SDA fAOT over Asia. One reason is that the MODIS DT
418 algorithm underestimates the FMF. Fig. S7-S10 shows the validation of the MODIS
419 FMF, and Table S3 summarizes the validation results. Most of the MODIS-derived
420 FMFs are below the 1:1 line due to the nil retrieval issue for MODIS FMF outputs.

Figure 10 shows that the yearly MODIS FMF is always between 0.5 and 0.6 in most areas of Asia. Even in Hebei Province in China where high levels of $PM_{2.5}$ pollution occur, the MODIS FMF still ranges from 0.5–0.6 in 2015 and 2016. However, the LUT-SDA FMF is greater than 0.7 in this region and also has high values (0.7–1.0) in many other provinces. Jethva et al. (2010) also found a similar underestimation of the MODIS-derived FMF in comparison with the AERONET FMF. The inaccuracy of MODIS-retrieved FMFs was reported by Levy et al. (2007). Using 780 pairs of collocated data at 200 AERONET stations, the linear regression relation between MODIS- and AERONET-derived FMF had a slope equal to1.051, a y-intercept equal to -0.347, and an R^2 equal to 0.248 (Levy et al., 2007). Note that the MODIS C6 FMF can equal zero (Fig. S7-S10), which was also noted by Jethva et al. (2010) and Suman et al. (2014).

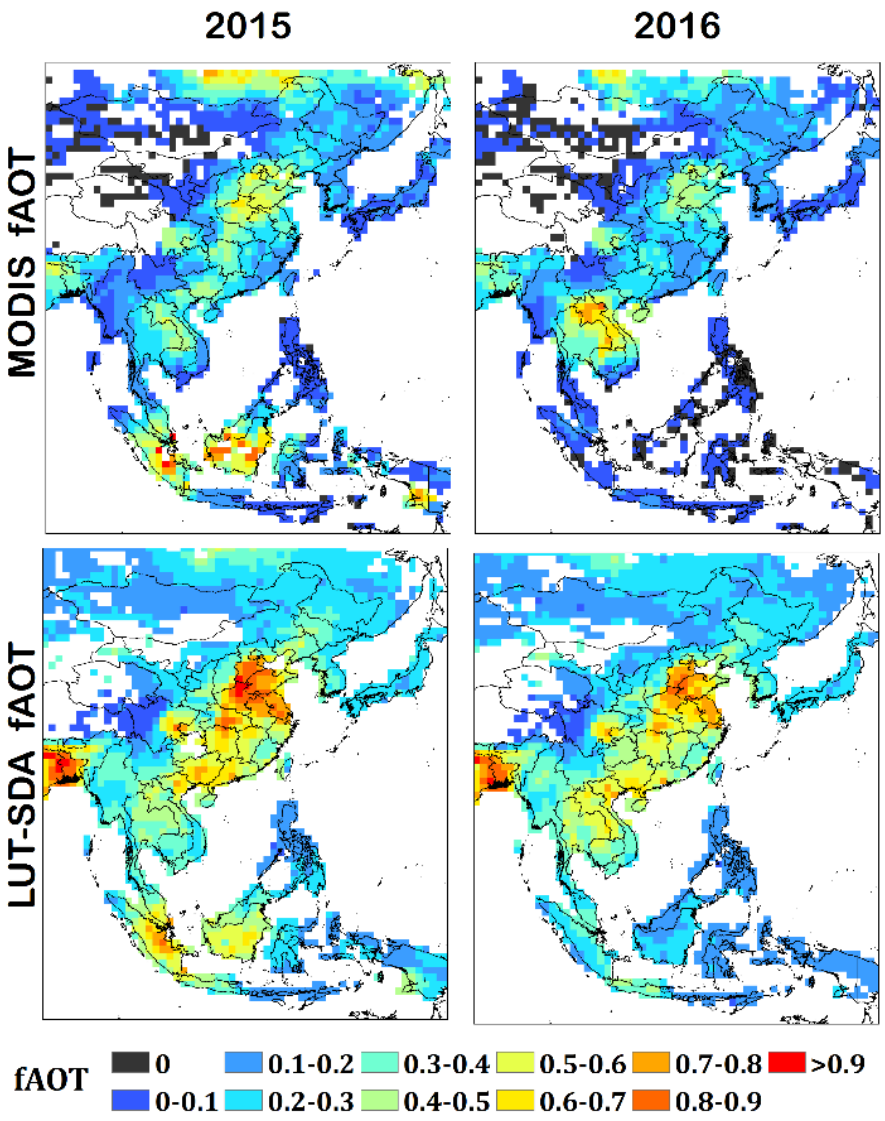

433

434 **Fig. 9.** Yearly averaged spatial distributions of fAOT in Asia from the MODIS DT

435 algorithm (top panels) and the LUT-SDA (bottom panels) for the years 2015

436 (left-hand panels) and 2016 (right-hand panels).

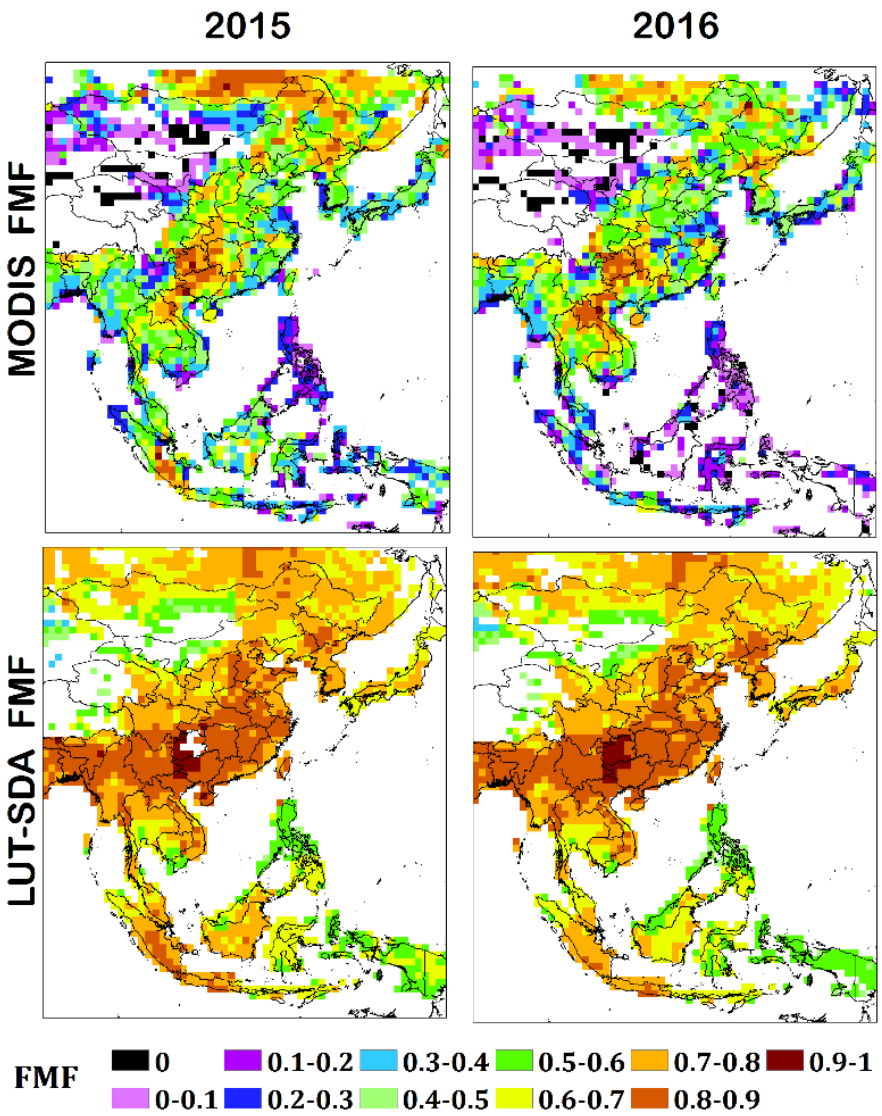

Fig. 10. Same as Fig. 6 but for the FMF.

Figure 11 shows LUT-SDA- and MODIS-derived fAOTs as a function of AERONET fAOT. High kernel density values show where most of the data lie. The MODIS-derived FMF has the smaller data volume because FMF data are provided only when the AOT quality assurance flag equals three. In order to compare their accuracies, redundant data were removed from the LUT-SDA dataset, and a new dataset was generated with the same data volume as the MODIS dataset (N=3807).

From Fig. 11, ~48% of LUT-SDA fAOT retrievals fall within the EE envelope. The linear regression relation has a slope equal to 0.91 and a y-intercept equal to 0.01 with an R^2 of 0.65 and an RMSE of 0.29. About 22% of the MODIS-derived fAOT points fall within the EE envelope while 64% of them are below the lower limit of the EE envelope due to the zero-value problem. The RMSE for the MODIS fAOT retrievals is 0.42 which is higher than that for the LUT-SDA fAOT retrievals. Overall, the LUT-SDA-derived FMFs agree well with AERONET retrievals, suggesting that the proposed retrieval method performs well.

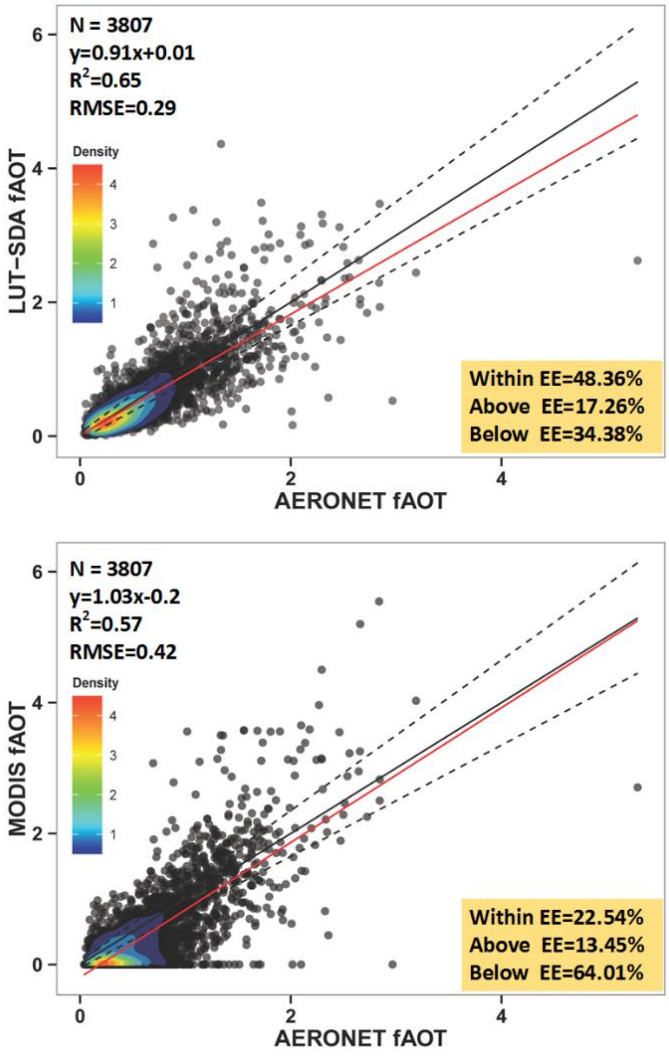

Fig. 11. LUT-SDA and MODIS fAOTs (at 500 nm) as a function of AERONET fAOT (at 500 nm). The red lines are the best-fit lines from linear regression, and the black solid lines are the 1:1 lines. The two dashed error lines are y = 1.15x + 0.05 (upper line) and y = 0.85x - 0.05 (bottom line) corresponding to the estimated error (EE) envelope ± (0.05 + 0.15 × AERONET fAOT). The regression equations and coefficients of determination (R^2) are given as well as the number of data points (N) and the root-mean-square errors (RMSE). Colored areas show the density of data points.

3.5. Discussion

In this study, we found a significant underestimation in MODIS fAOT retrievals compared with AERONET fAOT retrievals. This issue is consistent with the finding of Jethva et al. (2010) who found that the MODIS fAOT was underestimated in northern India (N=651, slope=0.44, and R^2=0.58). As shown in Figs. S7-S10, one reason for the underestimation lies in the existence of many zero or close-to-zero values in the MODIS-derived FMF. In addition, a considerable uncertainty with high RMSE between MODIS and AERONET FMFs was found in this study (Table S3), and this uncertainty was also reported by Lee and Chung (2013). Levy et al. (2007) pointed out that MODIS FMF retrievals are very sensitive to the choice of aerosol model. Jethva et al. (2010) and Suman et al. (2014) suggested that using a more absorbing aerosol type is better suited for fine-mode aerosols and can improve the retrieval accuracy in southern India. It is, however, not possible to constrain the

aerosol model from satellite information alone (Kokhanovsky et al., 2007). How to make a sound a priori assumption about the aerosol model is a major challenge which may be overcome to some extent by using ground-based measurements in different locations and seasons, as attempted in this and previous studies (O'Neill et al., 2001; Yan et al., 2017a).

The LUT-SDA can greatly improve the accuracy of fAOT retrievals, especially when using the update seasonal α' value. Compared with the previous annual α'-based LUT-SDA, the updated seasonal α'-based LUT-SDA improves the retrieval accuracy (Figs. 4–6). However, as shown in Fig. 5, there still are some uncertainties in the LUT-SDA FMF at low values (0–0.5). Since fAOT rather than total AOT is more closely linked to anthropogenic pollution sources (Bellouin et al., 2005), the more reliable fAOT retrieved by the LUT-SDA is a useful product to use for environmental research. Lee and Chung (2013) stated that the lack of reliable fine-mode aerosol data hinders the accurate estimation of global aerosol radiative forcing. Studies focused on the latter have used aerosol simulation models to distinguish natural aerosols from anthropogenic ones over land (Bellouin et al., 2005; Chung et al., 2005). To overcome this limitation, the LUT-SDA can serve as a useful and powerful tool for large-scale anthropogenic aerosol estimations.

The point of reducing the relative bias between MODIS FMFs and AERONET FMFs is to demonstrate the promising application of using FMFs to estimate $PM_{2.5}$. The estimation of ground-level $PM_{2.5}$ from satellite-derived AOT is fraught with uncertainties, a major one being the inability to retrieve FMF for fAOT which is more

499 closely related to $PM_{2.5}$ (Zhang and Li, 2013, 2015). Although the AERONET
500 FMF-based $PM_{2.5}$ retrieval model can significantly improve the $PM_{2.5}$ estimation
501 accuracy (Li et al., 2016; Yan et al., 2017b), the MODIS and AERONET FMFs are
502 defined differently and have a high bias between them. This limits the AERONET
503 FMF-based $PM_{2.5}$ retrieval model by using MODIS FMF for spatial $PM_{2.5}$ retrievals.
504 To remedy the problem, we have updated the LUT-SDA in this study to improve the
505 retrieval of fAOT by taking advantage of the climatology of regional aerosol
506 properties retrieved from AERONET (Eck et al., 2010).
507
508 **4. Conclusions**
509 In this study, an updated LUT-SDA for fAOT is presented and validated in Asia.
510 Based on five years of seasonal α' data from different AERONET locations
511 (2010–2014), we first updated the range of α' in the LUT-SDA to make this parameter
512 more in line with its seasonal characteristics. The comparison with the annual-based α'
513 LUT-SDA in Beijing, Hong Kong, and Osaka (Yan et al., 2017a) showed
514 improvements in the FMF retrievals for the three cities with the total mean RMSE
515 decreasing from 0.24 to 0.18. Improvements in fAOT retrievals can also be achieved
516 when using the updated LUT-SDA. The percentage of retrievals falling within the EE
517 envelope increases by 2.06, 3.67, and 7.30% for Beijing, Hong Kong, and Osaka,
518 respectively. The updated LUT-SDA was then applied to data from Asia and validated
519 by retrievals from 45 AERONET sites over the period of 2015–2016. The validation
520 showed that a good accuracy was achieved by the proposed method. More than half of

the updated LUT-SDA-derived fAOT retrievals at 31% of the sites and 40–50% of the retrievals at 42% of the sites fell within the EE envelope. Compared with the MODIS-derived C6 fAOT, a significant improvement in fAOT retrievals was achieved by the LUT-SDA. Using AERONET fAOT retrievals as baseline data, ~48% of LUT-SDA-based fAOT retrievals fell within the EE envelope (N=3807, RMSE=0.29), which is an improvement over that of the MODIS fAOT (~22% of the retrievals fell within the EE envelope, N=3807, RMSE=0.42). The fAOT was significantly underestimated by the MODIS algorithm in most areas of Asia with many unphysical values of zero. This study demonstrates that the refined LUT-SDA method is valid for the large-scale estimation of fAOT from satellite images.

Acknowledgements

This work was supported by the National Key Research and Development Plan of China (2017YFC1501702), the National Science Foundation of China (41675141, 41375155), and the Fundamental Research Funds for the Central Universities. The authors gratefully acknowledge the MODIS and AERONET teams for their effort in making the data available. The authors thank the reviewers for their constructive, detailed comments and suggestions related to this paper.

References

Arola, A., Eck, T.F., Kokkola, H., Pitkänen, M.R., Romakkaniemi, S., 2017. Assessment of cloud-related fine-mode AOD enhancements based on AERONET SDA product. Atmos. Chem. Phys. 17(9), 5991–6001. https://doi.org/10.5194/acp-17-5991-2017.

Beelen, R., and Coauthors, 2014. Effects of long-term exposure to air pollution on natural-cause mortality: an analysis of 22 European cohorts within the multicentre ESCAPE project. Lancet 383(9919), 785–795. https://doi.org/10.1016/S0140-6736(13)62158-3.

Bellouin, N., Boucher, O., Haywood, J., Reddy, M.S., 2005. Global estimates of aerosol direct radiative forcing from satellite measurements. Nature 438, 1138–1141. https://doi.org/10.1038/nature04348.

Chatterjee, A., Dutta, C., Jana, TK., Sen, S., 2012. Fine mode aerosol chemistry over a tropical urban atmosphere: characterization of ionic and carbonaceous species. J. Atmos. Chem. 69(2), 83–100. https://doi.org/10.1007/s10874-012-9231-8.

Cheng, Y., Su, H., Koop, T., Mikhailov, E., Pöschl, U., 2015. Size dependence of phase transitions in aerosol nanoparticles. Nature Comm. 6, 5923. https://doi.org/10.1038/ncomms6923.

Chung, C.E., Ramanathan, V., Kim, D., Podgorny, I.A., 2005. Global anthropogenic aerosol direct forcing derived from satellite and ground-based observations. J. Geophys. Res. Atmos. 110(D24). https://doi.org/10.1029/2005JD006356.

566 Csavina, J., Taylor, M.P., Félix, O., Rine, K.P., Sáez, A.E., Betterton, E.A., 2014.
567 Size-resolved dust and aerosol contaminants associated with copper and lead
568 smelting emissions: implications for emission management and human
569 health. Sci. Total Environ. 493, 750–756.
570 https://doi.org/10.1016/j.scitotenv.2014.06.031.
571 Dusek, U., Frank, G.P., Hildebrandt, L., Curtius, J., Schneider, J., Walter, S., Chand,
572 D., Drewnick, F., Hings, S., Jung, D., Borrmann, S., Andreae, M.O., 2006. Size
573 matters more than chemistry for cloud-nucleating ability of aerosol
574 particles. Science 312(5778), 1375–1378.
575 https://doi.org/10.1126/science.1125261.
576 Eck, T.F., Holben, B.N., Reid, J. S., Dubovik, O., Smirnov, A., O' Neill, N.T., Slutsker,
577 I., Kinne, S., 1999. Wavelength dependence of the optical depth of biomass
578 burning, urban, and desert dust aerosols. J. Geophys. Res. 104(D-24),
579 31,333–31,349. https://doi.org/10.1029/1999JD900923.
580 Eck, T.F., Holben, B.N., Sinyuk, A., Pinker, R.T., Goloub, P., Chen, H., Chatenet, B.,
581 Li, Z., Singh, R.P., Tripathi, S.N., Reid, J.S., Giles, D.M., Dubovik, O., O'Neill,
582 N.T., Smirnov, A., 2010. Climatological aspects of the optical properties of
583 fine/coarse mode aerosol mixtures. J. Geophys. Res. Atmos. 115, D19205.
584 https://doi.org/10.1029/2010JD014002.
585 Gao, Z.M., Jian-Rong, B.I., Huang, J.P., 2013. Analysis on aerosol optical property
586 over northern China from AERONET and SKYNET observations. Plateau
587 Meteor. 32(5), 1293–1307.

588 Gassó, S., O'Neill, N., 2006. Comparisons of remote sensing retrievals and in situ
589 measurements of aerosol fine mode fraction during ACE-Asia. Geophys. Res.
590 Let. 33(5). https://doi.org/10.1029/2005GL024926.
591 Gurjar, B.R., Jain, A., Sharma, A., Agarwal, A., Gupta, P., Nagpure, A.S., Lelieveld, J.,
592 2010. Human health risks in megacities due to air pollution. Atmos.
593 Environ. 44(36), 4606–4613. https://doi.org/10.1016/j.atmosenv.2010.08.011.
594 He, Q., Li, C., Tang, X., Li, H., Geng, F., Wu, Y., 2010. Validation of MODIS derived
595 aerosol optical depth over the Yangtze River Delta in China. Rem. Sens.
596 Environ. 114(8), 1649–1661. https://doi.org/10.1016/j.rse.2010.02.015.
597 Hubanks, P.A., King, M.D., Platnick, S., Pincus, R., 2008. MODIS Atmosphere L3
598 gridded product algorithm theoretical basis document. ATBD reference number:
599 ATBD-MOD-30, 30, pp 96.
600 Hubanks, P., Platnick, S., King, M.D., Ridgway, B., 2015. MODIS Atmosphere L3
601 gridded product algorithm theoretical basis document and users guide. ATBD
602 reference number: ATBD-MOD-30, NASA.
603 IPCC (Intergovernmental Panel on Climate Change), 2007. Climate Change 2007: the
604 Physical Science Basis: Contribution of Working Group I to the Fourth
605 Assessment Report of the Intergovernmental Panel on Climate Change.
606 IPCC (Intergovernmental Panel on Climate Change), 2013. Climate Change 2013: the
607 Physical Science Basis: Contribution of Working Group I to the Fifth Assessment
608 Report of the Intergovernmental Panel on Climate Change.
609 Itahashi, S., Uno, I., Yumimoto, K., Irie, H., Osada, K., Ogata, K., Fukushima, H.,

610 Wang, Z., Ohara, T., 2012. Interannual variation in the fine-mode MODIS
611 aerosol optical depth and its relationship to the changes in sulfur dioxide
612 emissions in China between 2000 and 2010. Atmos. Chem. Phys. 12(5),
613 2631–2640. https://doi.org/10.5194/acp-12-2631-2012.
614 Janjai, S., Nunez, M., Masiri, I., Wattan, R., Buntoung, S., Jantarach, T., Promsen, W.
615 (2012). Aerosol optical properties at four sites in Thailand. Atmos. Climate
616 Sci. 2(4), 441–453. https://doi.org/10.4236/acs.2012.24038.
617 Jethva, H., Satheesh, S. K., Srinivasan, J., 2007. Assessment of second-generation
618 MODIS aerosol retrieval (Collection 005) at Kanpur, India. Geophys. Res. Lett.
619 34(19). https://doi.org/10.1029/2007GL029647.
620 Jethva, H., Satheesh, S. K., Srinivasan, J., Levy, R.C., 2010. Improved retrieval of
621 aerosol size-resolved properties from moderate resolution imaging
622 spectroradiometer over India: role of aerosol model and surface reflectance. J.
623 Geophys. Res. Atmos. 115. https://doi.org/10.1029/2009JD013218.
624 Kaku, K.C., Reid, J.S., O'Neill, N.T., Quinn, P.K., Coffman, D.J., Eck, T.F., 2014.
625 Verification and application of the extended spectral deconvolution algorithm
626 (SDA+) methodology to estimate aerosol fine and coarse mode extinction
627 coefficients in the marine boundary layer. Atmos. Meas. Tech. 7(10), 3399–3412.
628 https://doi.org/10.5194/amt-7-3399-2014.
629 Kaskaoutis, D.G., Badarinath, K.V.S., Kumar Kharol, S., Rani Sharma, A.,
630 Kambezidis, H.D., 2009. Variations in the aerosol optical properties and types
631 over the tropical urban site of Hyderabad, India. J. Geophys. Res. 114, D22204.

https://doi.org/10.1029/2009JD012423.

Kaufman, Y.J., Boucher, O., Tanré, D., Chin, M., Remer, L.A., Takemura, T., 2005. Aerosol anthropogenic component estimated from satellite data. Geophys. Res. Lett. 32 (17). https://doi.org/10.1029/2005GL023125.

Kokhanovsky, A.A., 2009. Satellite aerosol remote sensing over land. G. Leeuw (Ed.). Berlin: Springer.

Kokhanovsky, A.A., Breon, F.M., Cacciari, A., 2007. Aerosol remote sensing over land: a comparison of satellite retrievals using different algorithms and instruments. Atmos. Res. 85 (3), 372-394. http://dx.doi.org/10.1016/j.atmosres.2007.02.008.

Kokhanovsky, A.A., Deuze, J.L., Diner, D.J., Dubovik, O., Ducos, F., Emde, C., Garay, M.J., Grainger, R.G., Heckel, A., Herman, M., Kastsev, I.L., Keller, J., Levy, R., North, P.R.J., Prikhach, A.S., Rozanov, V.V., Sayer, A.M., Ota, Y., Tanré, D., Thomas, G.E., Zege, E.P., 2010. The inter-comparison of major satellite aerosol retrieval algorithms using simulated intensity and polarization characteristics of reflected light. Atmos. Meas. Tech. 3, 909–932. https://doi.org/10.5194/amt-3-909-2010.

Lau, W.K.M., Yuan, C., Li, Z., 2018. Origin, maintenance and variability of the Asian Tropopause Aerosol Layer (ATAL): the roles of monsoon dynamics. Sci. Rep. 8(1), 3960–3960. https://doi.org/10.1038/s41598-018-22267-z.

Lee, K., Chung, C.E., 2013. Observationally-constrained estimates of global fine-mode AOD. Atmos. Chem. Phys. 13, 2907–2921.

https://doi.org/10.5194/acp-13-2907-2013.

Levy, R.C., Remer, L.A., Mattoo, S., Vermote, E., Kaufman, Y.J., 2007. Second-generation operational algorithm: retrieval of aerosol properties over land from inversion of Moderate Resolution Imaging Spectroradiometer spectral reflectance. J. Geophys. Res. Atmos. 112, D13211. http://dx.doi.org/10.1029/2006JD007811.

Levy, R.C., Remer, L.A., Kleidman, R.G., Mattoo, S., Ichoku, C., Kahn, R., Eck, T.F., 2010. Global evaluation of the Collection 5 MODIS dark-target aerosol products over land. Atmos. Chem. Phys. 10, 10,399–10,420. http://dx.doi.org/10.5194/acp-10-10399-2010.

Levy, R.C., Mattoo, S., Munchak, L.A., Remer, L.A., Sayer, A.M., Patadia, F., Hsu, N. C., 2013. The Collection 6 MODIS aerosol products over land and ocean. Atmos. Meas. Tech. 6, 2989–3034. https://doi.org/10.5194/amt-6-2989-2013.

Li, Z., Zhao, X., Kahn, R., Mishchenko, M., Remer, L.A., Lee, K.-H., Wang, M., Laszlo, I., Nakajima, T., Maring, H., 2009. Uncertainties in satellite remote sensing of aerosols and impact on monitoring its long-term trend: a review and perspective. Ann. Geophys. 27, 1–16. https://doi.org/10.5194/angeo-27-2755-2009.

Li, Z., and Coauthors, 2016. Remote sensing of atmospheric particulate mass of dry PM2.5 near the ground: method validation using ground-based measurements. Remote Sens. Environ. 173, 59–68. https://doi.org/10.1016/j.rse.2015.11.019.

Li, Z., Rosenfeld, D., Fan, J., 2017. Aerosols and their impact on radiation, clouds, precipitation, and severe weather events. Environ. Sci.

https://doi.org/10.1093/acrefore/9780199389414.013.126.

Luo, N., Wong, M.S., Zhao, W., Yan, X., Xiao, F., 2015. Improved aerosol retrieval algorithm using Landsat images and its application for PM10 monitoring over urban areas. Atmos. Res. 153, 264–275. https://doi.org/10.1016/j.atmosres.2014.08.012.

Ma, Z., Hu, X., Huang, L., Bi, J., Liu, Y., 2014. Estimating ground-level PM2.5 in China using satellite remote sensing. Environ. Sci. Technol. 48, 7436–7444. https://dx.doi.org/10.1021/es5009399.

Mielonen, T., Levy, R.C., Aaltonen, V., Komppula, M., de Leeuw, G., Huttunen, J., Lihavainen, H., Kolmonen, P., Lehtinen, K.E.J., Arola, A., 2011. Evaluating the assumptions of surface reflectance and aerosol type selection within the MODIS aerosol retrieval over land: the problem of dust type selection. Atmos. Meas. Tech. 4, 201–214. https://dx.doi.org/10.5194/amt-4-201-2011.

Mirante, F., Salvador, P., Pio, C., Alves, C., Artiñano, B., Caseiro, A., Revuelta, M.A., 2014. Size fractionated aerosol composition at roadside and background environments in the Madrid urban atmosphere. Atmos. Res. 138, 278–292. https://doi.org/10.1016/j.atmosres.2013.11.024.

O'Neill, N.T., Dubovik, O., Eck, T.F., 2001. Modified Ångström exponent for the characterization of submicrometer aerosols. Appl. Opt. 40, 2368–2375. https://doi.org/10.1364/AO.40.002368.

O'Neill, N.T., Eck, T.F., Smirnov, A., Holben, B.N., Thulasiraman, S., 2003. Spectral discrimination of coarse and fine mode optical depth. J. Geophys. Res. Atmos. 108(D17). https://doi.org/10.1029/2002JD002975.

O'Neill, N.T., Eck, T.F., Reid, J.S., Smirnov, A., Pancrati, O., 2008. Coarse mode optical information retrievable using ultraviolet to short-wave infrared Sun photometry: application to United Arab Emirates Unified Aerosol Experiment data. J. Geophys. Res. Atmos. 113(D5). https:// doi.org/10.1029/2007JD009052.

Pope III, C.A., Ezzati, M., Dockery, D.W., 2009. Fine-particulate air pollution and life expectancy in the United States. N. Engl. J. Med. 360, 376–386. https:// doi.org/10.1056/NEJMsa0805646.

Ramachandran, S., 2007. Aerosol optical depth and fine mode fraction variations deduced from Moderate Resolution Imaging Spectroradiometer (MODIS) over four urban areas in India. J. Geophys. Res. Atmos. 112(D16). https://doi.org/10.1029/2007JD008500.

Ruiz-Arias, J.A., Dudhia, J., Gueymard, C.A., Pozo-Vázquez, D., 2013. Assessment of the Level-3 MODIS daily aerosol optical depth in the context of surface solar radiation and numerical weather modeling. Atmos. Chem. Phys. 13(2), 675–692. https://doi.org/10.5194/acp-13-675-2013.

Soni, K., Singh, S., Bano, T., Tanwar, R. S., Nath, S., 2010. Variations in single scattering albedo and Ångström absorption exponent during different seasons over Delhi. Atmos. Environ. 44(35), 4355– 4363. https://doi.org/10.1016/j.atmosenv.2010.07.058.

Soni, K., Singh, S., Bano, T., Tanwar, R.S., Nath, S., 2011. Wavelength dependence of the aerosol Ångström exponent and its implications over Delhi, India. Aerosol Sci. Technol. 45, 1488–1498. https://doi.org/10.1080/02786826.2011.601774.

722 Suman, S., Gadhavi, H., Ravi Kiran, V., Jayaraman, A., Rao, S.V.B., 2014. Role of
723 coarse and fine mode aerosols in MODIS AOD retrieval: a case study over
724 southern India. Atmos. Meas. Tech. 7(4), 907–917.
725 https://doi.org/10.5194/amt-7-907-2014.
726 Tan, J., Duan, J., Zhen, N., He, K., Hao, J., 2016. Chemical characteristics and source
727 of size-fractionated atmospheric particle in haze episode in Beijing. Atmos. Res.
728 167, 24–33. https://doi.org/10.1016/j.atmosres.2015.06.015.
729 Wang, L., Xin, J., Wang, Y., Li, Z., Wang, P., Liu, G., Wen, T., 2007. Validation of
730 MODIS aerosol products by CSHNET over China. Chinese Sci. Bull. 52(12),
731 1708–1718. https://doi.org/10.1007/s11434-007-0222-0.
732 Wang, Y., Zhang, R., Saravanan, R., 2014. Asian pollution climatically modulates
733 mid-latitude cyclones following hierarchical modelling and observational
734 analysis. Nature Comm. 5. https://doi.org/10.1038/ncomms4098.
735 Xin, J., Zhang, Q., Wang, L., Gong, C., Wang, Y., Liu, Z., Gao, W., 2014. The
736 empirical relationship between the PM2.5 concentration and aerosol optical
737 depth over the background of North China from 2009 to 2011. Atmos. Res. 138,
738 179–188. https://doi.org/10.1016/j.atmosres.2013.11.001.
739 Yan, X., Shi, W. Z., Zhao, W.J., Luo, N.N., 2014. Impact of aerosols and atmospheric
740 particles on plant leaf proteins. Atmos. Environ. 88, 115–122.
741 https://doi.org/10.1016/j.atmosenv.2014.01.044.
742 Yan, X., Li, Z., Shi, W., Luo, N., Wu, T., Zhao, W., 2017a. An improved algorithm for
743 retrieving the fine-mode fraction of aerosol optical thickness. Part 1: Algorithm
744 development. Remote Sens. Environ. 192, 87–97.

https://doi.org/10.1016/j.rse.2017.02.005.

Yan, X., Shi, W., Li, Z., Li, Z., Luo, N., Zhao, W., Wang, H., Yu, X., 2017b. Satellite-based PM2.5 estimation using fine-mode aerosol optical thickness over China. Atmos. Environ. 170, 290–302. https://doi.org/10.1016/j.atmos.env.2017.09.023.

Yan, X., Li, Z., Luo, N., Shi, W., Zhao, W., Yang, X., Jin, J., 2018. A minimum albedo aerosol retrieval method for the new-generation geostationary meteorological satellite Himawari-8. Atmos. Res. 207, 14–27. https://doi.org/10.1016/j.atmosres.2018.02.021.

Yu, X., Zhu, B., Zhang, M., 2009. Seasonal variability of aerosol optical properties over Beijing. Atmos. Environ. 43(26), 4095–4101. https://doi.org/10.1016/j.atmosenv.2009.03.061.

Zhang, Y., Li, Z., 2013. Estimation of PM2.5 from fine-mode aerosol optical depth. J. Remote Sens. 17, 929–943.

Zhang, Y., Li, Z., 2015. Remote sensing of atmospheric fine particulate matter (PM 2.5) mass concentration near the ground from satellite observation. Remote Sens. Environ. 160, 252–262. https://doi.org/10.1016/j.rse.2015.02.005.

Zhang, Y., Wang, Y., Zhang, Y. H., Wei, P. W., Lü, Y., 2013. Improving accumulation-mode fraction based on spectral aerosol optical depth in Beijing. Spectrosc. Spect. Anal. 33(10), 2795–2802. https://doi.org/10.3964/j.issn.1000-0593(2013)10-2795-08.

Zheng, Y., Dong, Z., Wu, R., Li, Z., Jiang, H., 2011. Validation of MODIS aerosol optical thickness retrieval over the Yangtze Delta region of China. Advances in

Earth Science, 26(2), 224–234.

List of Figure Captions

Fig. 1. The study area. Colors represent the normalized difference vegetation index (NDVI), and the red dots show the locations of AERONET sites from which data are used in this study.

Fig. 2. Schematic diagram describing the LUT-SDA used in this study.

Fig. 3. Histograms of α' for different seasons at the (from top to bottom) Xinglong, Chiang_Mai_Met_Sta, Beijing, and Hong_Kong_PolyU AERONET sites. The red dashed line shows α' = 0.

Fig. 4. FMF error as a function of season for (A) Beijing, (B) Osaka, and (C) Hong Kong. The FMF error is defined as LUT-SDA-retrieved FMF – AERONET FMF. The red dashed line is the zero-error line, and the gray shaded area is the estimated error envelope (±0.1). The means, medians, and 66% (1-σ) intervals of the differences are shown as blue dots, horizontal lines within the boxes, and the boxes themselves, respectively. The black whiskers are the 96% (2-σ) intervals. D: RMSE of the LUT-SDA FMF in different seasons using seasonal and annual α' values.

Fig. 5. Box plots of FMF errors (LUT-SDA - AERONET) as a function of AERONET FMF at 0.5 μm for seasonal α'- and annual α'-based results for (A-B) Beijing, (C-D) Osaka, and (E-F) Hong Kong. The means, medians, and 66% (1-σ) intervals of the differences are shown as red dots, horizontal lines within the boxes, and the boxes

790 themselves, respectively. The blue whiskers are the 96% (2-σ) intervals. The black
791 dashed line is 0, and the red dashed lines represent the estimated error envelope for
792 the total FMF ± (0.05+15%).
793 **Fig. 6.** Updated (seasonal α'-based, left panels) and previous (annual α'-based, right
794 panels) LUT-SDA fAOTs collocated with 0.5-μm AERONET fAOTs. Data are sorted
795 according to ordered pairs (AERONET, LUT-SDA) of fAOT in 0.05 intervals, and the
796 color represents the number of cases (see color bars) having that particular
797 ordered-pair value. The 1:1 line and estimated error (EE) envelopes ± (0.05+15%) are
798 plotted in black solid and dashed lines, respectively. The red lines are the best-fit lines
799 from linear regression. The coefficients of determination (R^2), the number of samples
800 (N), and the root-mean-square errors (RMSE) are given in each panel.
801 **Fig. 7.** Seasonal mean fAOT from the LUT-SDA (background colors) and from
802 AERONET (colored filled circles).
803 **Fig. 8.** (A) Validation of the LUT-SDA fAOT (at 500 nm) in Asia at each site, (B)
804 MODIS as a function of AERONET AOT (at 500 nm) at Taihu, and (C) LUT-SDA
805 fAOT as a function of AERONET fAOT (at 500 nm) at Taihu. The solid black lines in
806 (B) and (C) are the 1:1 lines, the dotted black lines are the estimated error (EE)
807 envelope lines, and the red lines are the best-fit lines from linear regression. (D) Time
808 series of the LUT-SDA-derived FMF (in blue) and the Taihu AERONET FMF (in red)
809 from 2015 to 2016.
810 **Fig. 9.** Yearly averaged spatial distributions of fAOT in Asia from the MODIS DT
811 algorithm (top panels) and the LUT-SDA (bottom panels) for the years 2015

(left-hand panels) and 2016 (right-hand panels).

Fig. 10. Same as Fig. 6 but for the FMF.

Fig. 11. LUT-SDA and MODIS fAOTs (at 500 nm) as a function of AERONET fAOT (at 500 nm). The red lines are the best-fit lines from linear regression, and the black solid lines are the 1:1 lines. The two dashed error lines are $y = 1.15x + 0.05$ (upper line) and $y = 0.85x - 0.05$ (bottom line) corresponding to the estimated error (EE) envelope $\pm$ (0.05 + 0.15 $\times$ AERONET fAOT). The regression equations and coefficients of determination (R^2) are given as well as the number of data points (N) and the root-mean-square errors (RMSE). Colored areas show the density of data points.

Figure 1

Click here to download high resolution image

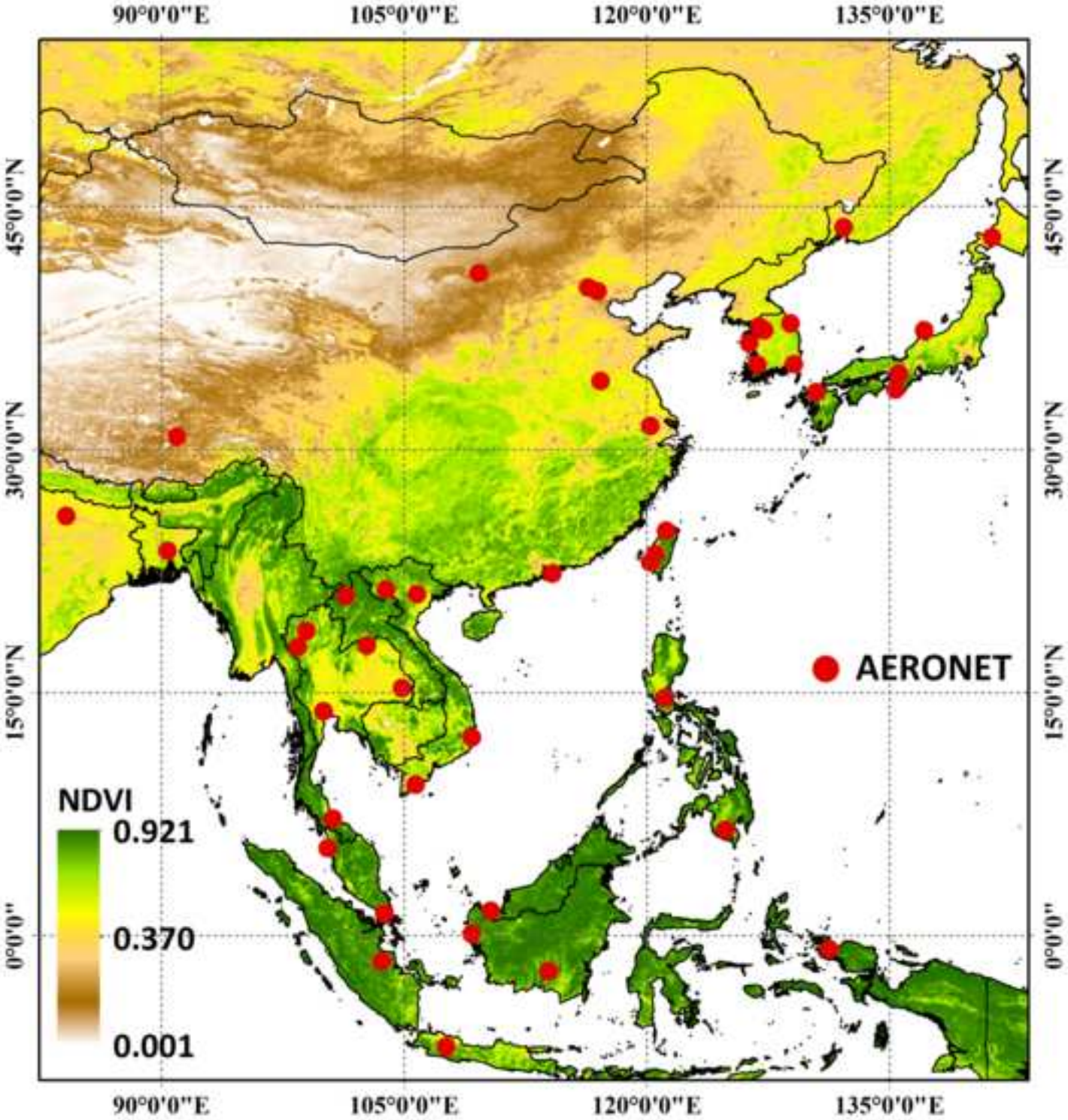

Figure 2

Click here to download high resolution image

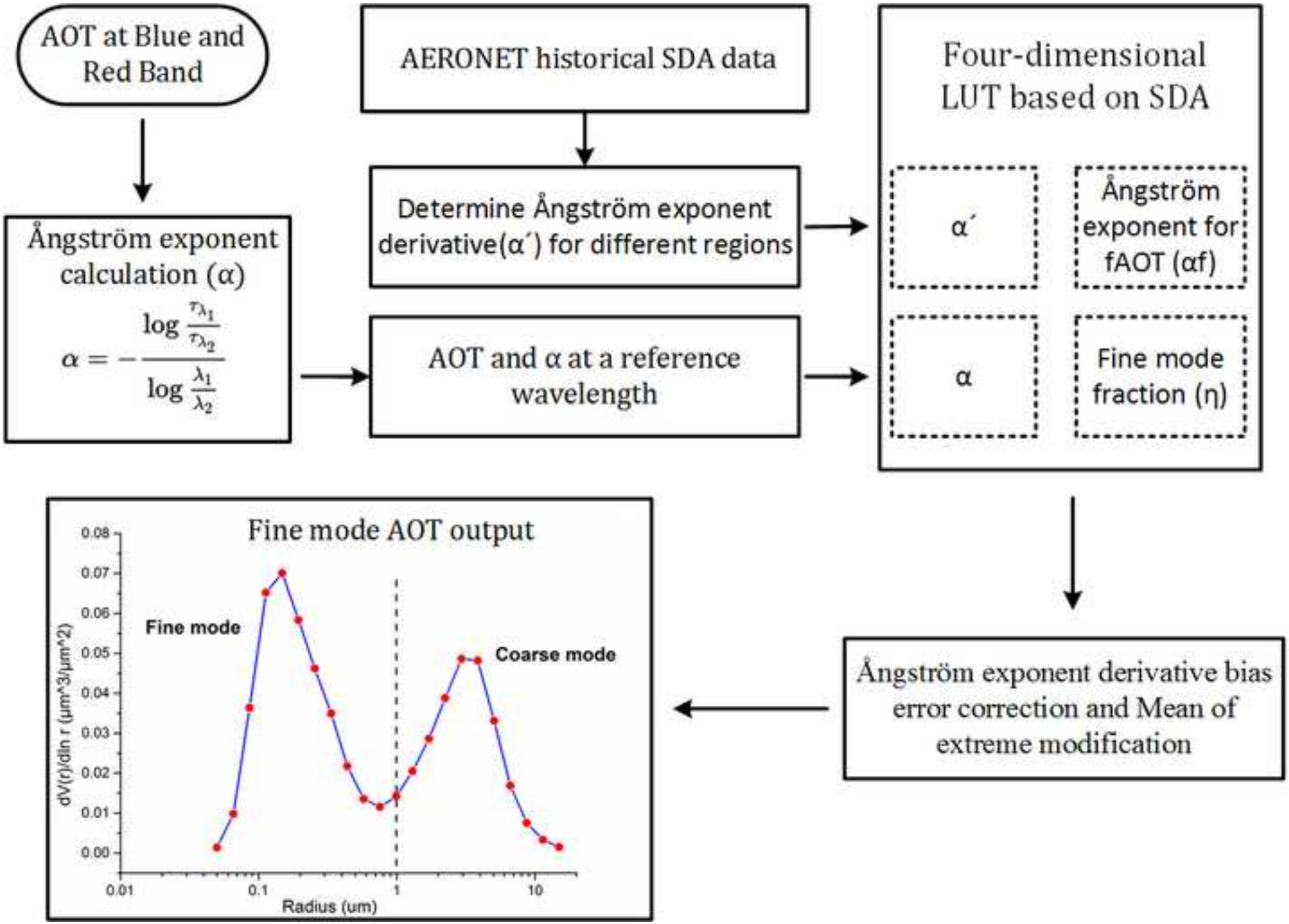

Figure 3

Click here to download high resolution image

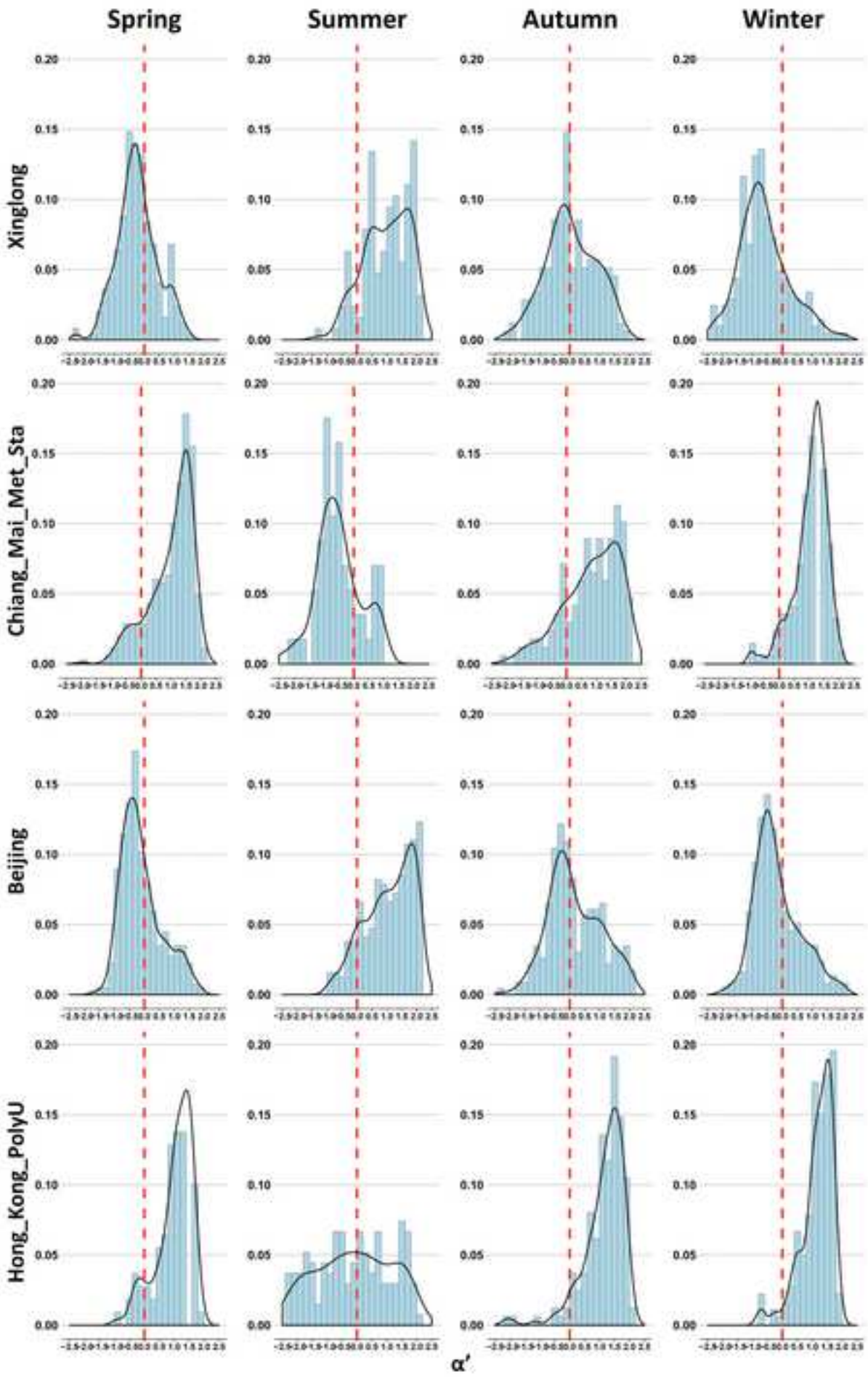

Figure 4

Click here to download high resolution image

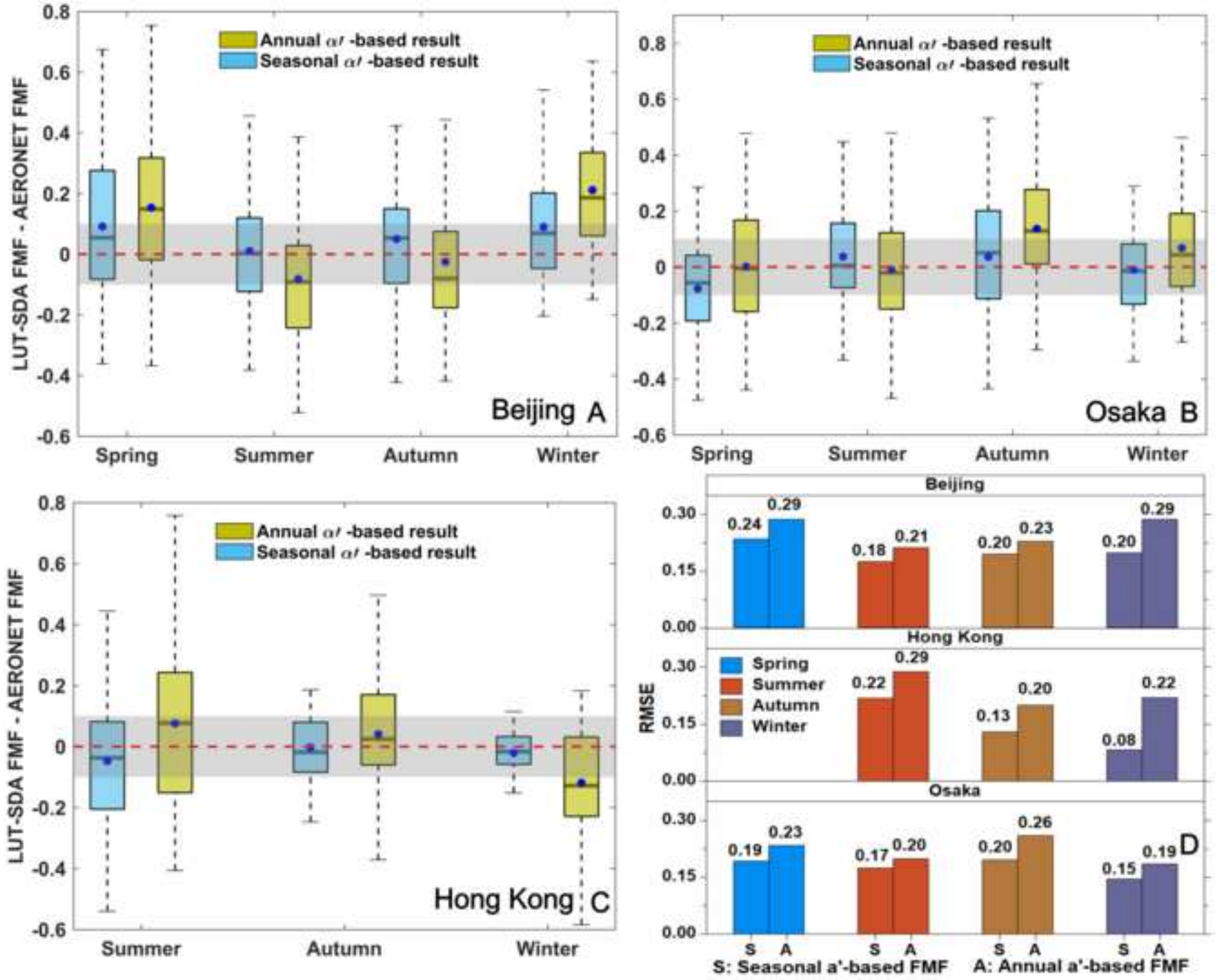

Figure 5

Click here to download high resolution image

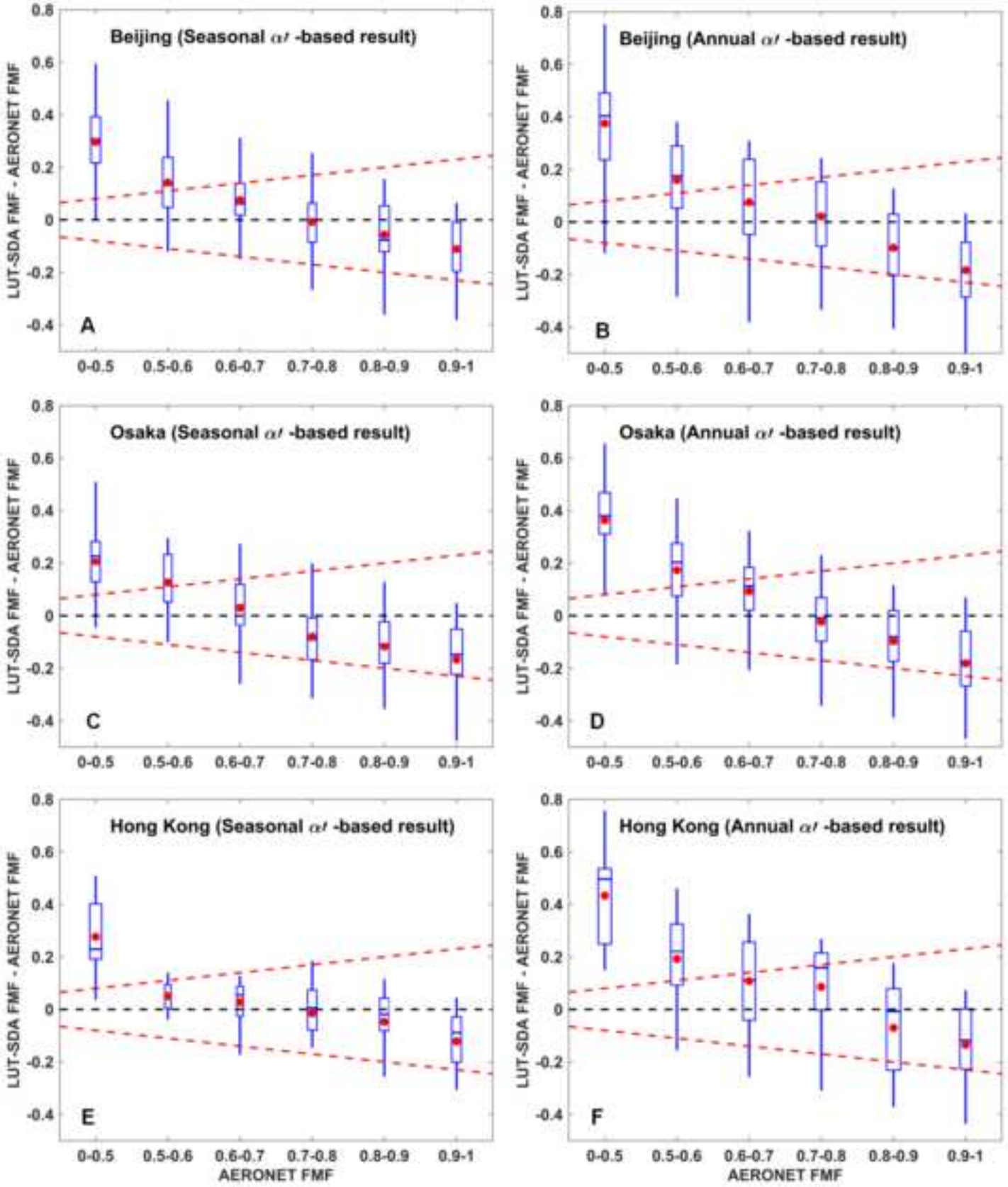

Figure 6

Click here to download high resolution image

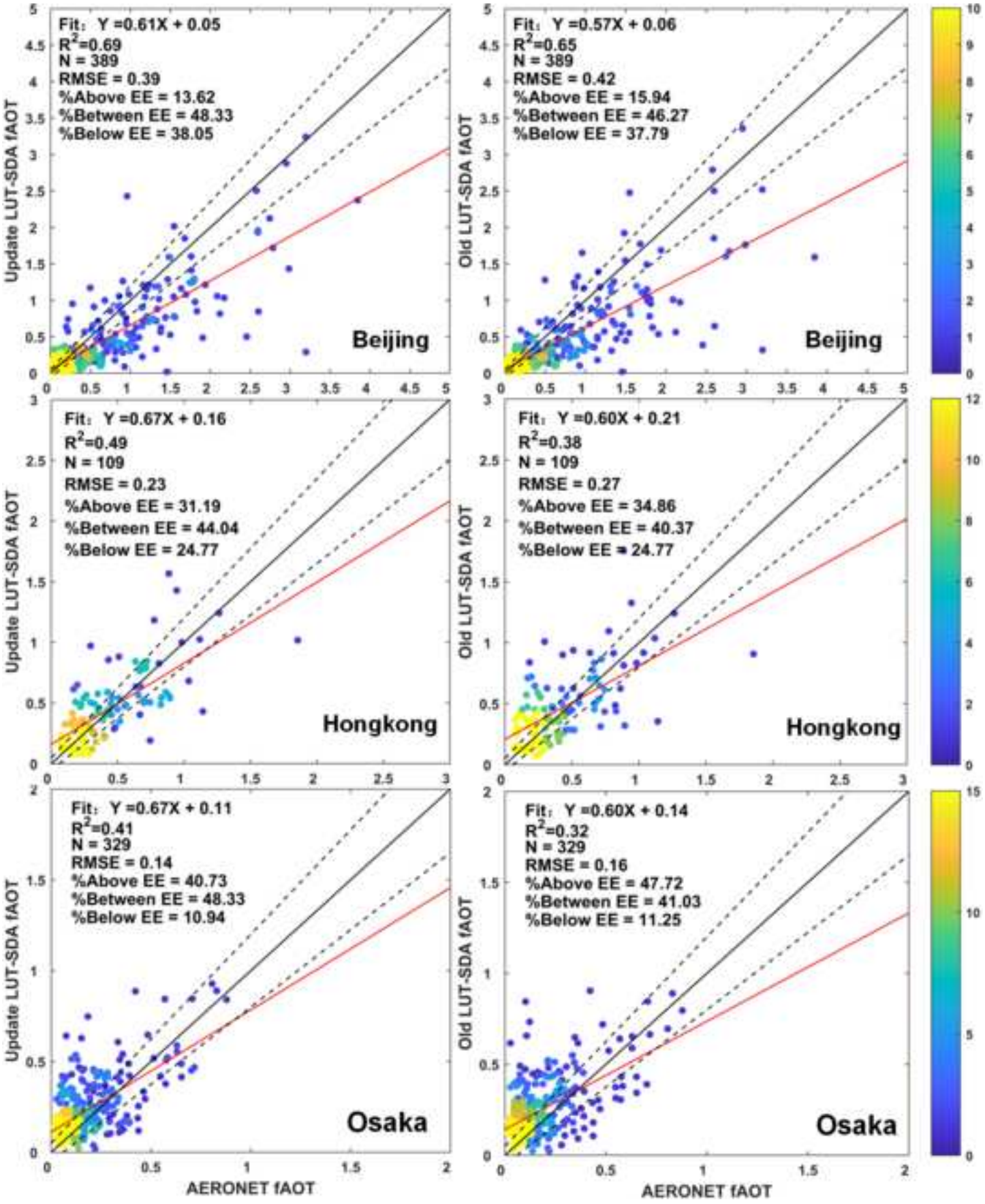

Figure 7

Click here to download high resolution image

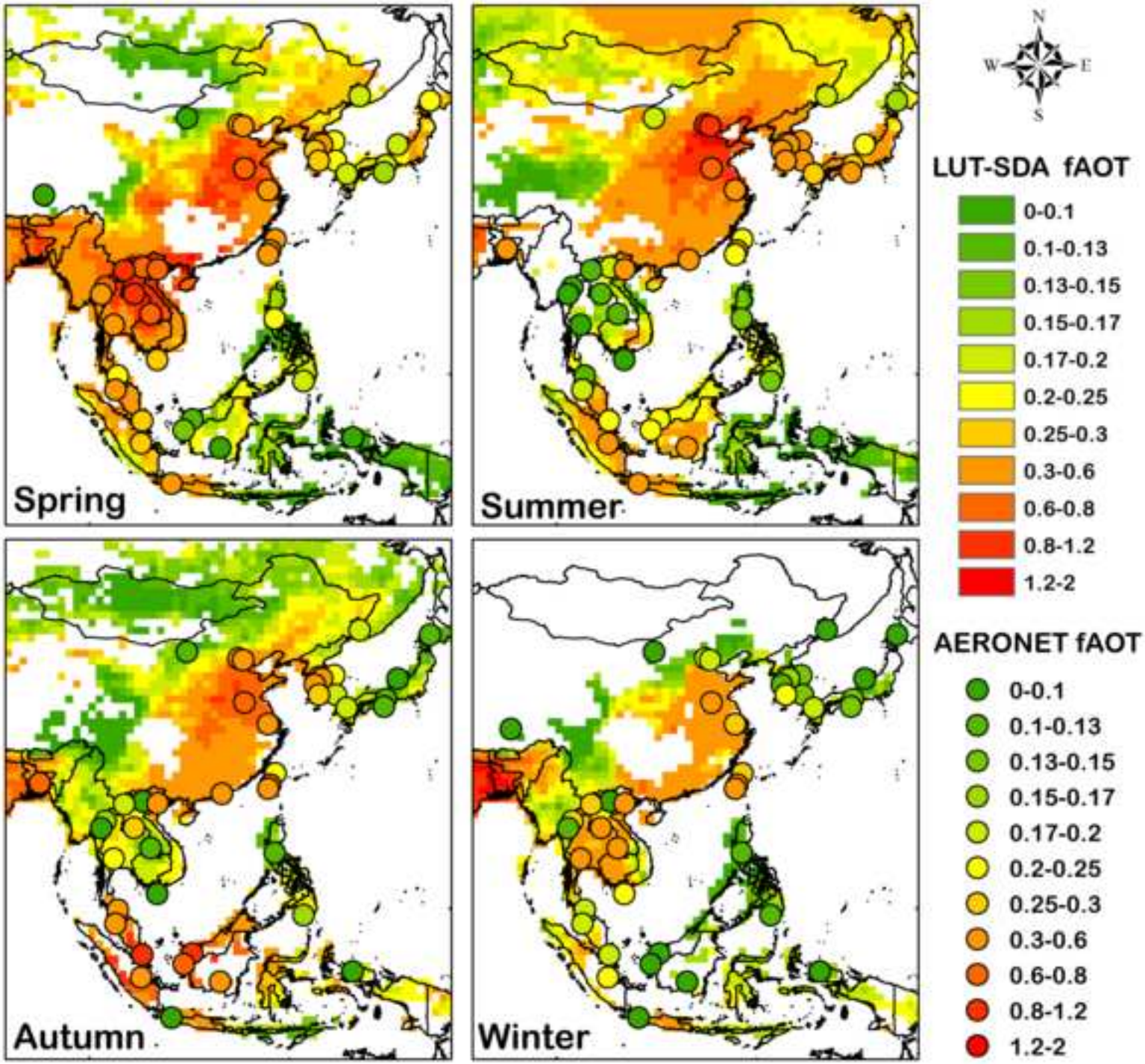

Figure 8

Click here to download high resolution image

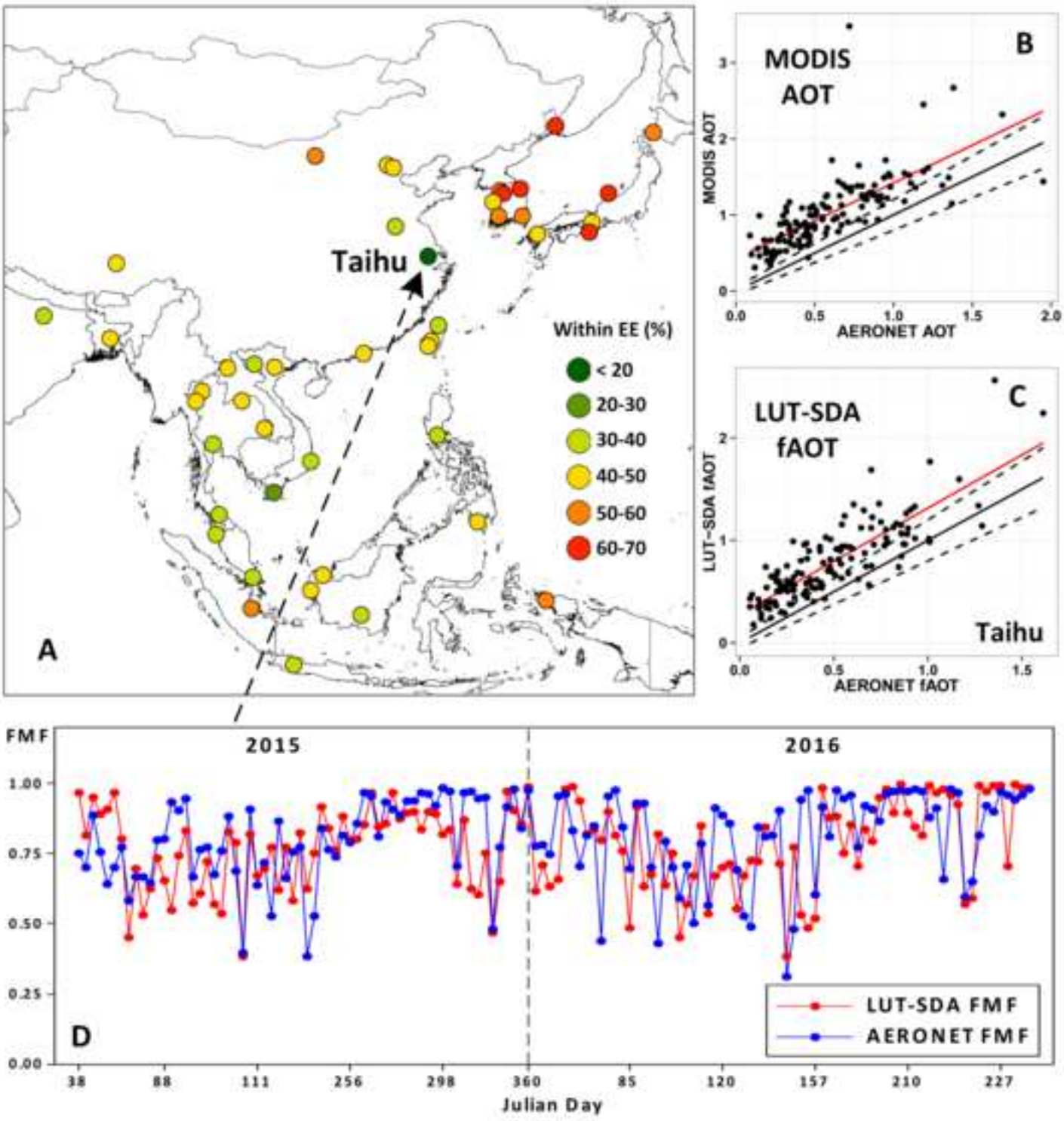

Figure 9

Click here to download high resolution image

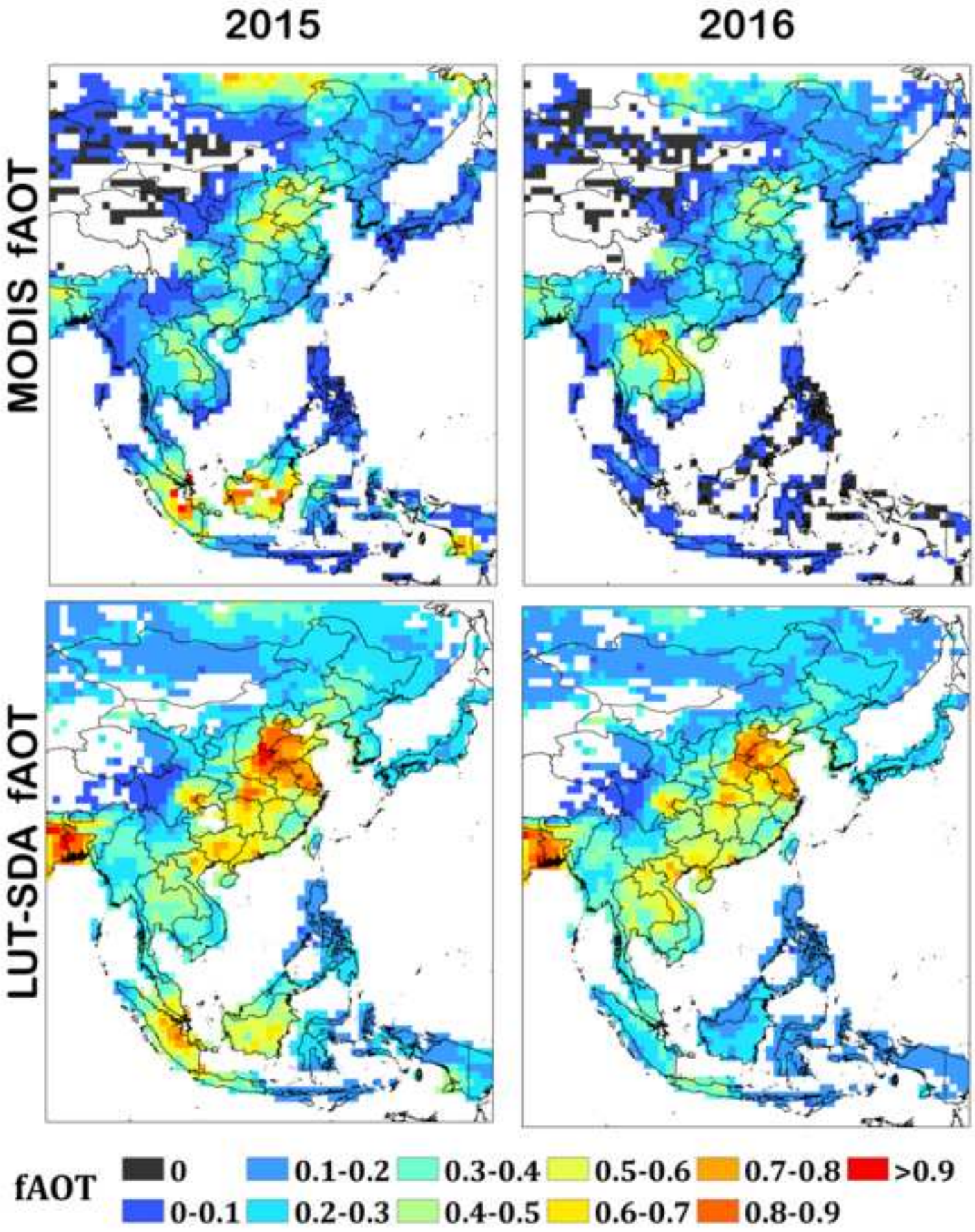

Figure 10

Click here to download high resolution image

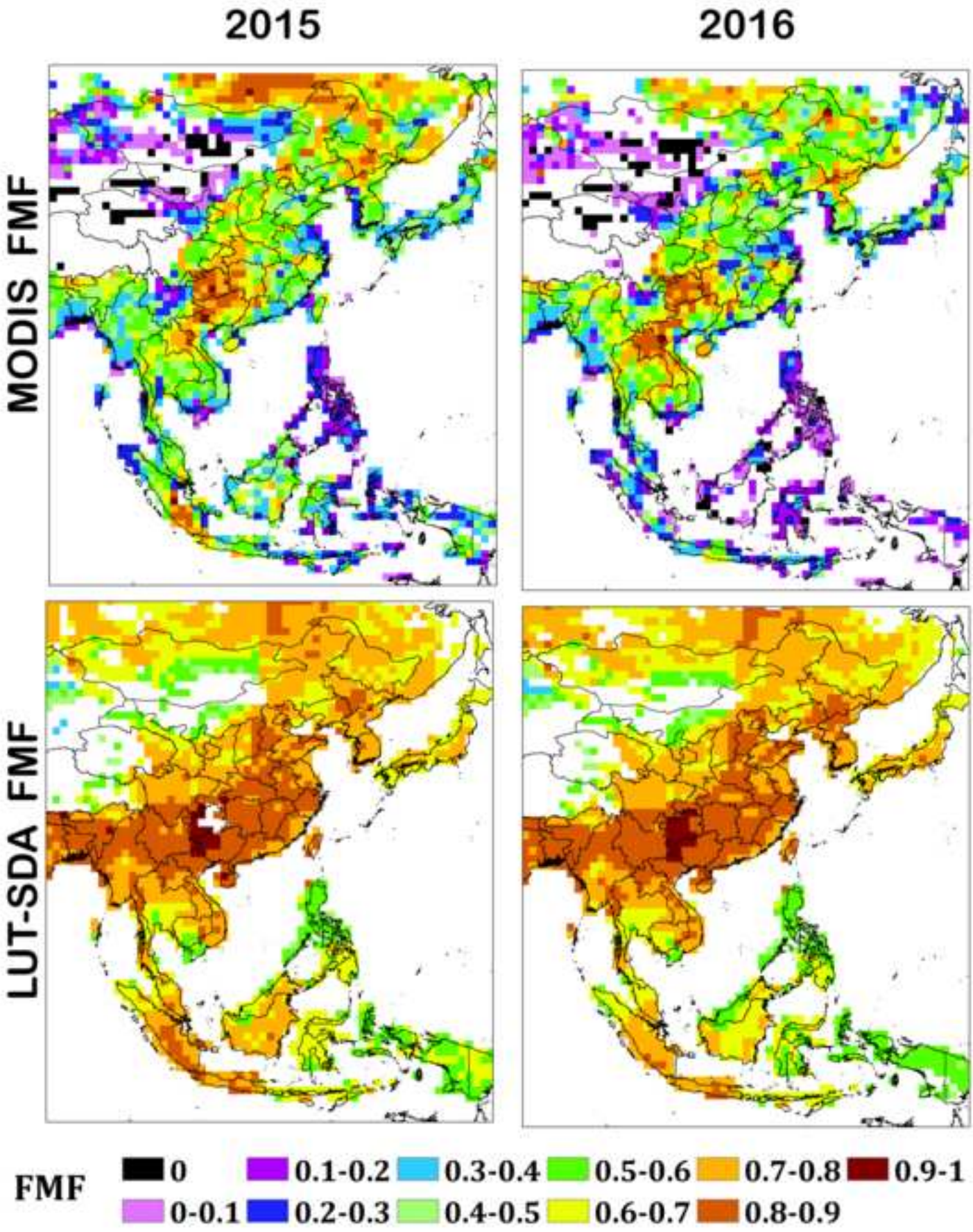

Figure 11

Click here to download high resolution image

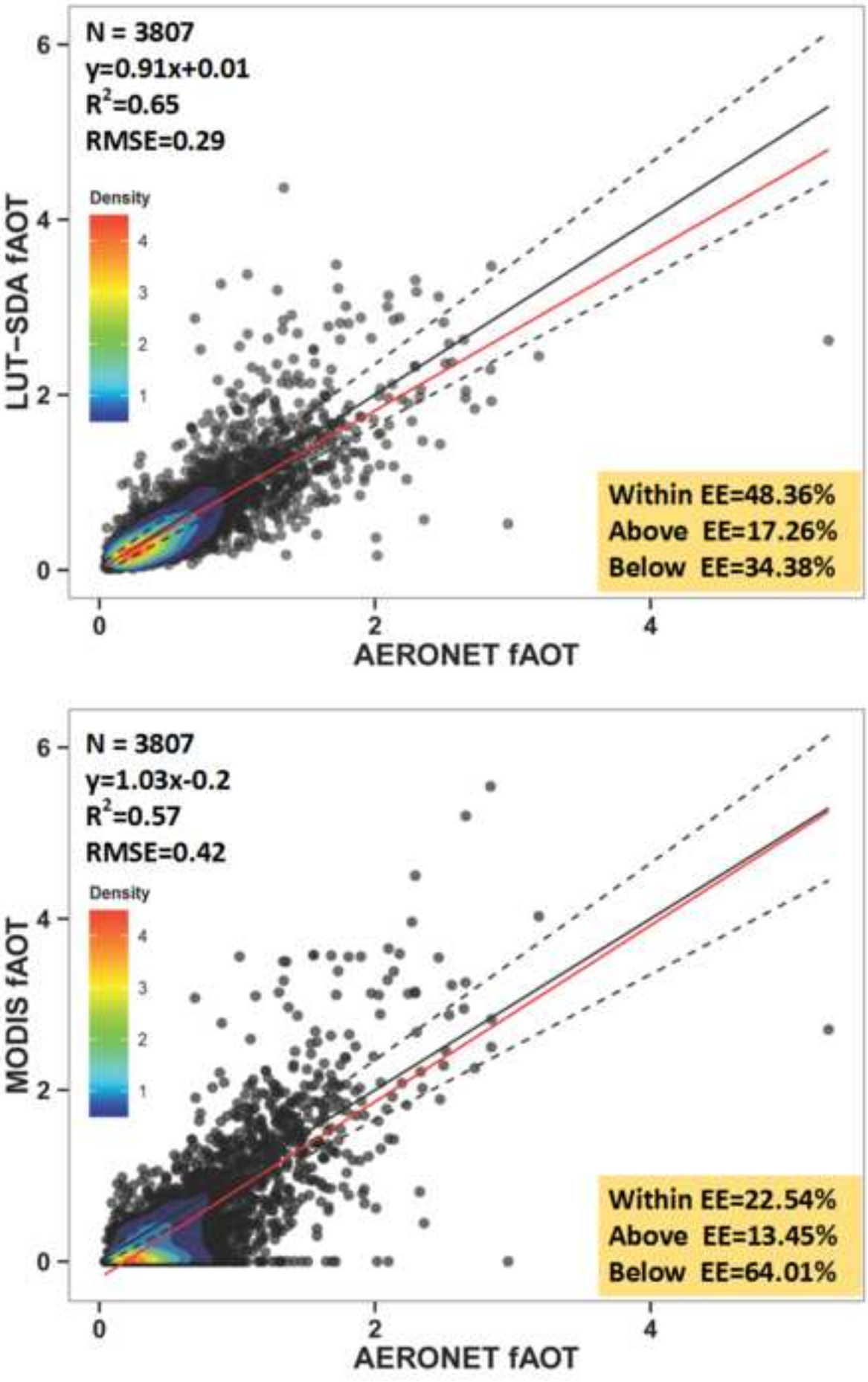

Supplementary Data

Click here to download Supplementary Data: Supplementary.docx